Table 1. Summary of the Structural Optimization Process for Quinolone Integrase Inhibitors[e]

	compd	Inhibition of Strand Transfer[a] IC_{50} (nM)	Antiviral Activity[b] EC_{50} (μM)	Cytotoxicity (μM)
7	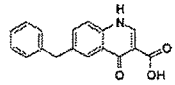	1600 ± 300	> 30000	> 30
8	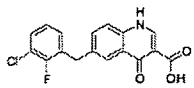	43.5 ± 8.8	805.2 ± 225.0	> 12
9	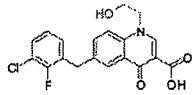	24.2 ± 11.6	76.3 ± 3.7	> 15
10	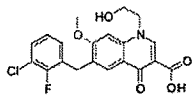	9.1 ± 2.1	17.1 ± 2.9	5.3 ± 1.1
11	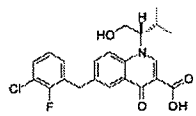	8.2 ± 1.7	7.5 ± 0.8	14.0 ± 2.0
12	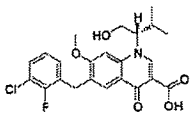	7.2 ± 2.2	0.9 ± 0.4	4.0 ± 0.8
5 (L-870,810)[c]		22.8 ± 4.3	3.6 ± 0.4	0.7 ± 0.06
Ciprofloxacin[d]		> 100000	–	–

[a] The strand transfer assay was performed according to the method of Hazuda[14] with some modifications.[15] [b] Antiviral activity was measured by the acute HIV-1 infection assay[16] with some modifications.[17] [c] Prepared according to the reported method.[18] [d] Available from Wako Pure Chemical [e] Data are given as the mean ± SD (n = 3).

replication (EC_{50} = 7.5 nM) than **9**, although introduction of an isopropyl group at the 1*R*-position of the hydroxyethyl moiety could not enhance inhibitory acitivity. Introduction of both a methoxy group at the 7-position of the quinolone ring and an isopropyl group at the 1*S*-position of the hydroxyethyl moiety of **9** (**12**) led to a synergistic improvement of antiviral acitivity (EC_{50} = 0.9 nM), but there was no additive or synergistic improvement in the inhibition of HIV-1 integrase (IC_{50} = 7.2 nM). This may be due to the condition of the strand transfer assay using 5 nM of target DNA that influences potencies of inhibitors.

Preparation of the quinolone analogues (**7**−**12**) is shown in Scheme 1. Palladium-catalyzed coupling of 3-chloro-2-fluorobenzylzinc bromide **13**, which was derived from the corresponding benzylbromide, with 1-iodo-4-nitrobenzene or 1-iodo-2-methoxy-4-nitrobenzene (Negishi coupling) and subsequent reduction of the nitro group gave the aniline **15** or **16**. Condensation of **15**, **16**, or commercially available **14** with diethyl ethoxymethylenemalonate and subsequent thermal cyclization of the aminoacrylate products in diphenyl ether led to the quinolone esters **17**, **18** and **19**.[19] Hydrolysis of **17** and **18** gave **7** and **8**, respectively. N-Alkylation of **18** or **19** with the *tert*-butyldimethylsilyl (TBS) ether of 2-hydroxyethylbromide and subsequent hydrolysis of the ethyl ester and TBS ether resulted in **9** or **10**. After 5-iodonation of 2-fluorobenzoic acids **20** and **21**, the acid chlorides of **20** and **21** were coupled with ethyl 3-(dimethylamino)acrylate to produce the acrylates **22** and

Scheme 1[a]

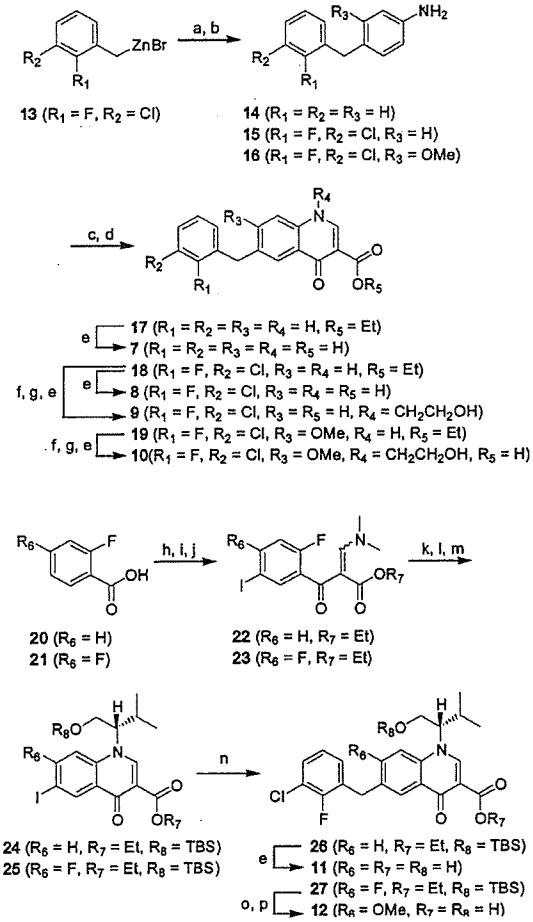

[a] Reagents and conditions: (a) 1-iodo-4-nitrobenzene, $PdCl_2(Ph_3P)_2$, THF, reflux; (b) Zn, AcOH; (c) diethyl ethoxymethylenemalonate, toluene, reflux; (d) Ph_2O, 250 °C; (e) NaOH, EtOH/H_2O, reflux; (f) $TBSOCH_2CH_2Br$, K_2CO_3, DMF, 80 °C; (g) TBAF, THF; (h) NIS, H_2SO_4; (i) $SOCl_2$, DMF, toluene, reflux; (j) ethyl 3-(dimethylamino)acrylate, THF, 50 °C; (k) (*S*)-valinol, THF; (l) K_2CO_3, DMF, 70 °C; (m) TBSCl, imidazole, DMF; (n) **13**, $Pd(dba)_2$, trifurylphosphine, THF, reflux; (o) NaOH, *i*-PrOH/H_2O, reflux; (p) NaOMe, MeOH, reflux.

23, respectively. Substitution with (*S*)-valinol and subsequent cyclization with potassium carbonate and protection of the alcohol with TBS ether gave the quinolones **24** and **25**, respectively.[20] Negishi coupling of **24** and **25** with **13** led to the quinolone esters **26** and **27**, respectively. Hydrolysis of **26** gave **11**. Hydrolysis of **27** and subsequent methoxylation with sodium methoxide produced **12**.

In summary, modification of quinolone antibiotics, which did not show HIV-1 integrase inhibitory activity (Table 1), led to discovery of the coplanar monoketo acid motif in their scaffold, 4-quinolone-3-carboxylic acid, as an alternative to the diketo acid motif. These novel quinolone integrase inhibitors were structurally optimized in the highly potent **12**, which had little antibacterial activity although it still retained the core structure of quinolone antibiotics. Compound **12** was much more potent at inhibiting integrase-catalyzed strand transfer processes than 3′-processing reactions, as previously reported for compounds of the diketo acid class.[12,13] This indicates that it probably inhibits HIV-1 integrase via a mechanism similar to that of diketo acids, although there is no direct evidence (such as cocrystal data) that the coplanar monoketo acid motif shows the same mode of binding to the enzyme as the diketo acid

motif. Clinical studies of the novel quinolone integrase inhibitor **12** (GS 9137) are currently being conducted by Gilead Sciences.

Acknowledgment. We thank H. Isoshima and K. Kondo for sample preparation; S. Kato for comments on the manuscript; and S. Ishiguro, J. Haruta, and M. Kano for support.

Supporting Information Available: Analytical data for **5** and **7**−**12**. This material is available free of charge via the Internet at http://pubs.acs.org.

References

(1) Pommier, Y.; Johnson, A. A.; Marchand, C. Integrase inhibitors to treat HIV/AIDS. *Nat. Rev. Drug Discovery* **2005**, *4*, 236−248.
(2) Craigie, R. HIV integrase, a brief overview from chemistry to therapeutics. *J. Biol. Chem.* **2001**, *276*, 23213−23215.
(3) Richman, D. D. HIV chemotherapy. *Nature* **2001**, *410*, 995−1001.
(4) Weiss, R. A. HIV and AIDS: looking ahead. *Nat. Med.* **2003**, *9*, 887−891.
(5) Johnson, A. A.; Marchand, C.; Pommier, Y. HIV-1 integrase inhibitors: a decade of research and two drugs in clinical trial. *Curr. Top. Med. Chem.* **2004**, *4*, 1059−1077.
(6) Barreca, M. L.; Ferro, S.; Rao, A.; Luca, L. D.; Zappala, M.; Monforte, A. M.; Debyser, Z.; Witvrouw, M.; Chimirri, A. Pharmacophore-based design of HIV-1 integrase strand-transfer inhibitors. *J. Med. Chem.* **2005**, *48*, 7084−7088.
(7) Hazuda, D. J.; Young, S. D.; Guare, J. P.; Anthony, N. J.; Gomez, R. P.; Wai, J. S.; Vacca, J. P.; Handt, L.; Motzel, S. L.; Klein, H. J.; Dornadula, G.; Danovich, R. M.; Witmer, M. V.; Wilson, K. A. A.; Tussey, L.; Schleif, W. A.; Gabryelski, L. S.; Jin, L.; Miller, M. D.; Casimiro, D. R.; Emini, E. A.; Shiver, J. W. Integrase inhibitors and cellular immunity suppress retroviral replication in rhesus macaques. *Science* **2004**, *305*, 528−532.
(8) Grobler, J. A.; Stillmock, K.; Binghua, H.; Witmer, M.; Felock, P.; Espeseth, A. S.; Wolfe, A.; Egbertson, M.; Bourgeois, M,; Melamed, J.; Wai, J. S.; Young, S.; Vacca, J.; Hazuda, D. J. Diketo acid inhibitor mechanism and HIV-1 integrase: implications for metal binding in the active site of phosphotransferase enzymes. *Proc. Natl. Acad. Sci. U.S.A.* **2002**, *99*, 6661−6666.
(9) Goldgur, Y.; Craigie, R.; Cohen, G. H.; Fujiwara, T.; Yoshinage, T.; Fujishita, T.; Sugimoto, H.; Endo, T.; Murai, H.; Davies, D. R. Structure of the HIV-1 integrase catalytic domain complexed with an inhibitor: a platform for antiviral drug design. *Proc. Natl. Acad. Sci. U.S.A.* **1999**, *96*, 13040−13043.
(10) Hazuda, D. J.; Anthony, N. J.; Gomez, R. P.; Jolly, S. M.; Wai, J. S.; Zhuang, L.; Fisher, T. E.; Embrey, M.; Guare, J. P., Jr.; Egbertson, M. S.; Vacca, J. P.; Huff, J. R.; Felock, P. J.; Witmer, M. V.; Stillmock, K. A.; Danovich, R.; Grobler, J.; Miller, M. D.; Espeseth, A. S.; Jin, L.; Chen, I. W.; Lin, J. H.; Kassahun, K.; Ellis, J. D.; Wong, B. K.; Xu, W.; Pearson, P. G.; Schleif, W. A.; Cortese, R.; Emini, E.; Summa, V.; Holloway, M. K.; Young, S. D. A naphthyridine carboxamide provides evidence for discordant resistance between mechanistically identical inhibitors of HIV-1 integrase. *Proc. Natl. Acad. Sci. U.S.A.* **2004**, *101*, 11233−11238.
(11) Zhuang, L.; Wai, J. S.; Embrey, M. W.; Fisher, T. E.; Egbertson, M. S.; Payne, L. S.; Guare, J. P., Jr.; Vacca, J. P.; Hazuda, D. J.; Felock, P. J.; Wolfe, A. L.; Stillmock, K. A.; Witmer, M. V.; Moyer, G.; Schleif, W. A.; Gabryelski, L. J.; Leonard, Y. M.; Lynch, J. J., Jr.; Michelson, S. R.; Young, S. D. Design and synthesis of 8-hydroxy-[1,6]naphthyridines as novel inhibitors of HIV-1 integrase in vitro and in infected cells. *J. Med. Chem.* **2003**, *46*, 453−456.
(12) Hazuda, D. J.; Felock, P.; Witmer, M.; Wolfe, A.; Stillmock, K.; Grobler, J. A.; Espeseth, A.; Gabryelski, L.; Schleif, W.; Blau, C.; Miller, M. D. Inhibitors of strand transfer that prevent integration and inhibit HIV-1 replication in cells. *Science* **2000**, *287*, 646−650.
(13) Sechi, M.; Derudas, M.; Dallocchio, R.; Dessi, A.; Bacchi, A.; Sannia, L.; Carta, F.; Palomba, M.; Ragab, O.; Chan, C.; Shoemaker, R.; Sei, S.; Dayam, R.; Neamati, N. Design and synthesis of novel indole β-diketo acid derivatives as HIV-integrase inhibitors, *J. Med. Chem.* **2004**, *47*, 5298−5310.
(14) Hazuda, D. J.; Hastings, J. C.; Wolfe, A. L.; Emini, E. A. A novel assay for the DNA strand-transfer reaction of HIV-1 integrase. *Nucleic Acids Res.* **1994**, *22*, 1121−1122.
(15) Donor DNA (which was processed at the 3′ end of the strand and biotinylated at the 5′ end) was immobilized on streptavidin-coated microtiter plates. Recombinant integrase (300 nM) was assembled on the immobilized donor DNA (0.5 pmol per well) in 100 μL of reaction buffer (30 mM 3-(*N*-morpholino)propanesulfonic acid (MOPS), 5 mM $MgCl_2$, 3 mM dithiothreitol (DTT), 0.1 mg/mL bovine serum albumin (BSA), 5% glycerol, 10% DMSO, 0.01% Tween-20) by incubation for 60 min at 37 °C. Then excess enzyme was removed and a test compound was added. The strand transfer reaction was initiated by addition of target DNA (5 nM), which was labeled at the 3′ end with digoxigenin. After incubation at 37 °C for 10 min, the plates were washed with phosphate-buffered saline (PBS) containing 0.1% Tween-20. The digoxigenin-labeled products were detected using anti-digoxigenin-peroxidase (POD) Fab fragments (Roche Diagnostics) and a POD substrate, tetramethylbenzidine (TMB). Then 100 μL of anti-digoxigenin-POD Fab fragment solution was added to each well, and the plates were incubated at 37 °C for 60 min. After the mixture was washed with PBS containing 0.1% Tween-20, 100 μL of the POD substrate (TMB) was added to each well, and the plates were incubated at room temperature. The colorimetric reaction was stopped by addition of 100 μL of 0.5 M H_2SO_4, and the absorbance was measured at 450 nm by a microplate reader (SPECTRA max 340, Molecular Devices).
(16) Pauwels, R.; Balzarini, J.; Baba, M.; Snoeck, R.; Schols, D.; Herdewijn, P.; Desmyter, J.; De Clercq, E. Rapid and automated tetrazolium-based colorimetric assay for the detection of anti-HIV compounds. *J. Virol. Methods* **1988**, *20*, 309−321.
(17) MT-4 human T lymphoid cells (1×10^5 cells/mL) in RPMI 1640 medium containing 10% fetal bovine serum, 100 U/mL penicillin, and 100 μg/mL streptomycin were infected with HIV-1 strain IIIb at a multiplicity of 0.01 and were distributed into 96-well microtiter plates. Test compounds were added to the wells, and cultures were incubated at 37 °C for 5 days. Cell viability was determined by the MTT assay, which measures living cells on the basis of mitochondrial dehydrogenase activity. The cells were incubated with 3-(4,5-dimethylthiazol-2-yl)-2,5-diphenyltetrazolium bromide (MTT) solution (7.5 mg/mL). The MTT formazan crystals were dissolved in acidic 2-propanol containing 4% Triton-X, and the absorbance was measured at 595 nm.
(18) Anthony, N. J.; Gomez, R. P.; Young, S. D.; Egbertson, M.; Wai, J. S.; Zhuang, L.; Embrey, M.; Tran, L.; Melamed, J. Y.; Langford, H. M.; Guare, J. P.; Fisher, T. E.; Jolly, S. M.; Kuo, M. S.; Perlow, D. S.; Bennett, J. J.; Funk, T. W. Aza- and polyaza-naphthalenyl carboxamides useful as HIV integrase inhibitors. PCT Int. Appl. WO02/30930 A2, 2002 (Merck & Co., Inc.).
(19) Gould, R. G., Jr.; Jacobs, W. A. The synthesis of certain substituted quinolines and 5,6-benzoquinolines. *J. Am. Chem. Soc.* **1939**, *61*, 2890−2895.
(20) Cecchetti, V.; Fravolini, A.; Lorenzini, M. C.; Tabarrini, O.; Terni, P.; Xin, T. Studies on 6-aminoquinolones: synthesis and antibacterial evaluation of 6-amino-8-methylquinolones. *J. Med. Chem.* **1996**, *39*, 436−445.

JM0600139

Nucleic Acids Symposium Series No. 50 1–2
doi:10.1093/nass/nrl001

2'-Deoxy-4'-C-ethynyl-2-fluoroadenosine: A nucleoside reverse transcriptase inhibitor with highly potent activity against all HIV-1 strains, favorable toxic profiles and stability in plasma

Hiroshi Ohrui[1], Satoru Kohgo[2], Hiroyuki Hayakawa[2], Eiichi Kodama[3], Masao Matsuoka[3], Tomohiro Nakata[4] and Hiroyuki Mitsuya[4,5]

[1]Yokohama College of Pharmacy, Yokohama, Japan, [2]Yamasa Corporation, Chiba, Japan, [3]Institute for Virus Research, Kyoto, Japan, [4]Kumamoto University, School of Medicine, Kumamoto, Japan and [5]National Cancer Institute/National Institute of Health, Bethesda, Maryland, USA

ABSTRACT

A working hypothesis to solve the critical problems of existing HAART was proposed. The study based on the hypothesis proved the validity of the hypothesis and resulted in the development of 2'-deoxy-4'-*C*-ethynyl-2-fluoro-adenosine (4'Ed2FA), a nucleoside reverse transcriptase inhibitor (NRTI) with highly potent activity against all HIV-1 strains, very favourable toxic profiles, and stability in plasma.

INTRODUCTION

HAART has dramatically improved the q. o. l. and prognosis of patients infected with HIV-1. However, the existing HAART has critical problems. They are
1) emergence of drug-resistant HIV variants,
2) requirement of frequent and large doses of drugs,
3) side effects of drugs.
A working hypothesis to solve the problems was proposed based on the fundamentals of both organic chemistry and biochemistry, and past findings of relationship between biological activity and structure of nucleoside derivatives. The hypothesis is comprised of the following three ways.

1) The way to prevent emergence of drug-resistant HIV
All clinical **NRTIs** belong to the family of 2',3'-dideoxy-nucleoside (**ddN**). The **ddN** structure has been assumed essential for nucleoside derivative to be anti-HIV active, i.e. to be the chain terminator of proviral DNA biosynthesis. However, HIV variants resistant to all these clinical **NRTIs** emerged. Resistance to these **ddNs** means that HIV can acquire the ability to discriminate between **ddN** and physiologic 2'-deoxynucleoside (**dN**) and does not accept **ddN** into the active center of its reverse transcriptase (RT) and /or selectively cut off the incorporated **ddN** from its proviral DNA terminus. Thus, resistance is the discrimination by HIV. Therefore, the nucleoside (N) that could prevent the emergence of drug-resistant HIV variants must satisfy the following conditions.

(1) To prevent discrimination by HIV, **N** must have the structure very much like **dN**. Therefore, **N** must have 3'-OH.
(2) In spite of having 3'-OH, **N** must be the chain terminator of proviral DNA biosynthesis.
2'-deoxy-4'-*C*-substitutednucleoside (**4'SdN**) was designed as the nucleoside that can satisfy these conditions on the basis of the following hypothesis.
(a) It will be difficult for HIV to discriminate between **4'SdN** and **dN** because **4'SdN** has all the functional groups of **dN**.
(b) The neopentyl-type secondary 3'-OH of **4'SdN** would be too unreactive to be used for elongation of proviral DNA biosynthesis. Thus, **4'SdN** could be the chain-terminator of proviral DNA biosynthesis.

2) The way to decrease the toxicity of nucleosides
In 1960s and 1970s, organic chemists synthesized nucleoside derivatives modified at two or more than two positions of physiologic nucleosides expecting to get nucleoside derivatives with excellent biological activity. However, none of them showed remarkable biological activity. These results suggested that the intracellular important enzymes do not recognize these modified nucleosides as their substrates. Therefore, the toxicity of **4'SdN** could be decreased by additional modification.

3) The way to provide nucleosides with stability to both enzymatic and acidic glycolysis
The lone pair of the ring oxygen plays an important role in both enzymatic and acidic glycolysis of nucleosides by participating to form an oxocarbonium ion. The steric hindrance between the 4'-substituent and 3'-OH of **4'SdN** changes the ring conformation into 3'-endo (N-type). It will be difficult for the lone pair of the ring oxygen of **4'SdN** with 3'-endo conformation to form oxocarbonium ion because the three bonds, C4-O-C1-C2, can not be co-planar easily. Thus, the introduction of a substituent at the 4'-position of nucleosides provide them with stability to both enzymatic and acidic glycolysis.

RESULTS AND DISCUSSION

Studies based on the hypothesis have proved the validity of the hypothesis. Optimization of the 4'-substituents, bases, and their combinations has resulted in the development of 2'-deoxy-4'-*C*-ethynyl-2-fluoroadenosine (**4'Ed2FA**, a nucleoside modified at two positions (4' and 2) of physiologic deoxyadenosine, which is highly active against all existing HIV strains has low toxicity, and is stable to both enzymatic and acidic glycolysis.

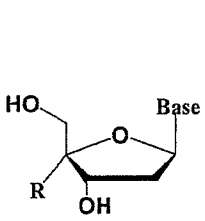

4'SdN

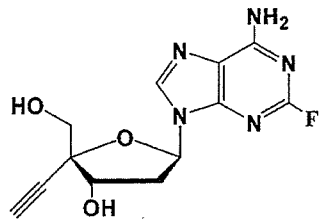

4'Ed2FA

The results of the biological evaluation of 4'Ed2FA

1) Anti-HIV activity:

EC_{50} (wild type)=0.2 nM; AZT=22 nM, (MDR)=0.14 nM; AZT=15,300 nM, (M184V)=3.1 nM; AZT=10 nM .

2) Toxicity:

DNA polymerase α: IC_{50}>200 μM,

DNA polymerase β: IC_{50}>200 μM,

Human mitochondrial DNA polymerase γ : IC_{50}=10 μM.

ddA: IC_{50}=0.2 μM

Mouse Toxicity: No acute toxicity up to 100 mg/kg by both oral and intravenous administration.

3) Stability to enzymatic and acidic glycolysis

Half life time of triphosphate of 4'Ed2FA: $T_{1/2}$: ~18hr,

triphosphate of AZT: $T_{1/2}$= 3hr

About 50% of the cells were protected against the infection of HIV-1 for 24 hr after removal of extracellular **4'Ed2FA** in both MT4 cells and MAGI cells cultured in the presence of 0.1 μM of **4'Ed2FA**.

Completely stable to adenosine deaminase under the conditions where **4'EdA** was completely deaminated within 60 min.

Only a small part (3 %) was hydrolyzed under the acidic Conditions of gastric juice (pH 1.06) at 24 °C, while **ddA** was completely decomposed in 5 min.

SUMMARY

A study on the synthesis and biological evaluation of **4'SdNs** was conducted according to a proposed hypothesis based on the fundamentals of both organic chemistry and biochemistry. Old findings proved the validity of the hypothesis and resulted in the development of **4'Ed2FA**, which is highly potent against all HIV-1s, is stable to intracellular catabolism and acidic degradation, has a very long intracellulat $T_{1/2}$, does not greatly inhibit DNA polymerase γ and does not have acute mouse toxicity. These results strongly suggest that **4'Ed2FA** deserves further study for the development of a highly potent therapeutic agent for HIV infection (**AIDS**), which may solve the problems of the existing HAART.

In addition, it should be noted that **4'Ed2FA** could be the ideal drug for both HIV and HBV infections. Hepatitis B virus (HBV) is a DNA virus, however, it also belongs to the family of retrovirus because it uses reverse transcriptase (**RT**) when it replicates. It was found that the **NRTIs** of HIV are also active against HBV, and **3TC** has been used for HBV infection.[9,10] However, HBV resistant to **3TC** has emerged. Since **4'Ed2FA** is highly active against 3TC-resistant HIV and will prevent the emergence of drug-resistant HIV, it is also expected to be active against drug-resistant HBV. Thus, **4'Ed2FA** could be the ideal drug for use against both HIV and HBV.

REFERENCES

1. Waga, T., Ohrui, H., Meguro, H. (1996) *Nucleosides Nucleotides,* **57,** 287.
2. Yamaguchi, T., Tomikawa, A., Hirai, T., Kawaguchi, T., Ohrui, H., Saneyoshi, M. (1997) *Nucleosides Nucleotides,* **16,** 1347.
3. Ohrui, H., Kohgo, S., Kitano, K., Sakata, S., Kodama, E., Yoshimura, K., Matsuoka, M., Shigeta, S., Mitsuya, H. (2001) *J. Med. Chem.*, **65,** 1879.
4. Kodama, E., Kohgo, S., Kitano, K., Machida, H., Gatanaga, H., Shigeta, S., Matsuoka, M., Ohrui, H., Mitsiya, H. (2001) *Antimicrobial Agents & Chemotherapy*, **45,** 1539.
5. Ohrui, H., Mitsuya, H. (2001) *Current Drug Targets-Infectious Disorder*, **1,** 1.
6. Kohgo, S., Yamada, K., Kitano, K., Iwai, Y., Sakata, N., Hayakawa, H., Nameki, D., Kodama, E., Matsuoka, M., Ohrui, H., Mitsuya, H. (2004) *Nucleosides Nucleotides*, **23,** 671.
7. Patent: International Publication Number, WO2005/090349, PCT/JP2005/005374
8. Nakata, H., Amano, M., Koh, Y., Kodama, E., Yang, G., Kohgo, S., Hayakawa, H., Ohrui, H., Matsuoka, M., Mitsuya, H. (2006) Abstract of 13th Conference on Retroviruses and Opportunistic Infections (CRO), F (antiviral therapy-preclinical), p219 (poster).
9. Lai, C. L., Dienstag, J., Schiff, E., Leung, N. W. Y., Akins, M., Hunt, C., Brown, N., Woessner, M., Boehme, R., Condreay, L. (2003) *Clin. Infect. Dis.*, **36,** 687.
10. Villeneuve, J. P., Durantel, D., Durantel, S., Westland, C., Xiong, S., Brosgart, C. L., Bibbs, C. S., Parvas, P., Nerle, B., Trepo, C., Zoulim, F. J. (2003) *Heptol.*, **39,** 1085.

Structure−Activity Relationships of Cyclic Peptide-Based Chemokine Receptor CXCR4 Antagonists: Disclosing the Importance of Side-Chain and Backbone Functionalities

Satoshi Ueda,[†] Shinya Oishi,[†] Zi-xuan Wang,[‡] Takanobu Araki,[†] Hirokazu Tamamura,[†,#] Jérôme Cluzeau,[†] Hiroaki Ohno,[†] Shuichi Kusano,[∥] Hideki Nakashima,[∥] John O. Trent,[§] Stephen C. Peiper,[‡] and Nobutaka Fujii[†,*]

Graduate School of Pharmaceutical Sciences, Kyoto University, Sakyo-ku, Kyoto 606-8501, Japan, Department of Pathology, Medical College of Georgia, Georgia 30912, Institute of Biomaterials and Bioengineering, Tokyo Medical and Dental University, Chiyoda-ku Tokyo 101-0062, Japan, St. Marianna University, School of Medicine, Miyamae-ku, Kawasaki 216-8511, Japan, and James Graham Brown Cancer Center, University of Louisville, Kentucky 40202

Received June 19, 2006

Previously, we have identified a highly potent CXCR4 antagonist **2** [cyclo(-D-Tyr[1]-Arg[2]-Arg[3]-Nal[4]-Gly[5]-)] and its Arg[2] epimer **3** [cyclo(-D-Tyr[1]-D-Arg[2]-Arg[3]-Nal[4]-Gly[5]-)] by the screening of cyclic pentapeptide libraries that were designed based on the structure−activity relationship studies on 14-residue peptidic CXCR4 antagonist **1**. In the present study, a new series of analogues of **2** and **3** were synthesized to evaluate the influences of peptide side-chain and backbone modification on bioactivities. Based on the Ala-scanning study, in which each residue in **2** and **3** was replaced with Ala having the identical chirality, substitution of Arg[3] and Nal[4] [Nal = L-3-(2-naphthyl)alanine] with Ala (compounds **6**, **7**, **10**, **11**) led to significant loss of the potency, indicating these amino acids are more important contributors to the bioactivity. For the cyclic peptide backbone, several modifications including D/L-Ala or cyclic amino acids substitution at the Gly[5] position and sequential *N*-methylation on amide nitrogens were conducted. Among the analogues, compounds **13** [cyclo(-D-Tyr[1]-Arg[2]-Arg[3]-Nal[4]-D-Ala[5]-)] and **32** [cyclo(-D-Tyr[1]-D-MeArg[2]-Arg[3]-Nal[4]-Gly[5]-)] were close in potency to the most potent lead **2**. NMR and conformational analysis indicated that both of these analogues favor the same backbone conformation as **2**, whereas similar analysis of less potent analogues indicates that an altered backbone conformation is favored. The conformational analysis showed that steric repulsion by a 1,3-allylic strain-like effect across the planar peptide bond might contribute to the conformational preferences of cyclic pentapeptides.

Introduction

Chemokines comprise a protein family of chemotactic factors that bind G protein-coupled receptors.[1,2] Engagement of chemokine receptors by their ligands triggers changes of the receptor conformation that lead to the initiation of a signaling cascade involving G protein binding, protein kinase activation, Ca^{2+} mobilization from intracellular stores, and cytoskeletal rearrangement, eventually leading to directed cell migration toward the gradients of the respective ligand.[3,4] A chemokine receptor CXCR4 and its endogenous ligand CXCL12 (stromal cell derived factor-1, SDF-1) are partners in multiple important functions in normal physiology involving the leukocyte chemotaxis in the immune system[5] and progenitor cell migration during embryologic development of the cardiovascular,[6,7] hemopoietic,[8] and central nervous systems.[9,10] On the other hand, CXCR4 has also multiple functions in pathologic physiology. CXCR4 serves as a coreceptor for infection of T cell line-tropic (X4) strains of the human immunodeficiency virus type 1 (HIV-1[a]). Following activation of the gp120 subunits of the envelope glycoprotein by binding to CD4, CXCR4 leads to membrane fusion and subsequent entry of the viral genome into the target cell.[11,12] Recently, Müller et al. disclosed that CXCL12/CXCR4 interactions participate in breast cancer metastasis analogous to programming directed migration in normal leukocytes and progenitor cells.[13] Expression of CXCR4 is enriched on the surface of malignant primary breast cancer cells while CXCL12 is preferentially expressed in organs that are frequent sites of metastasis in breast cancer, such as lung, liver, lymph nodes, and bone marrow. The coordinate actions between an attractant molecule and the corresponding receptor allow tumor cells to spread specifically to distant organs that provide a supportive niche. Furthermore, Nanki et al. reported that CXCL12/CXCR4 interactions might play a central role in memory T cell migration into inflamed rheumatoid arthritis (RA) synovium and for persisting inflammation at the affected site mediated by $CD4^+$ T cells.[14]

Thus, CXCR4 is considered as an important therapeutic target for multiple diseases. Several potent CXCR4 antagonists have been developed so far. Among them, a β-sheet-like 14-residue peptide **1** was identified by potency optimization of a 18-residue cyclic peptide isolated from horseshoe crabs (Figure 1).[15] The peptide **1** and its analogues were also characterized as HIV-1 entry inhibitors,[16] anticancer-metastatic,[17,18] and anti-RA agents.[19] Several other low-molecular-weight CXCR4 antagonists such as AMD3100[20,21] and KRH1636[22] have also been reported to inhibit HIV-1 infection through CXCR4. Recently, we have identified novel potent CXCR4 antagonists **2** and **3** by screening of two orthogonal cyclic pentapeptide libraries,[23] which were designed based on the structure−activity relationship studies on **1** (Figure 1).[24] These peptides contain two arginine, one 3-(2-naphthyl)alanine, and one tyrosine residue, that potentially

* Corresponding author. Tel: +81-75-753-4551, Fax: +81-75-753-4570, E-mail: nfujii@pharm.kyoto-u.ac.jp
† Kyoto University.
‡ Medical College of Georgia.
# Tokyo Medical and Dental University.
∥ St. Marianna University.
§ University of Louisville.

[a] Abbreviations: Nal, L-3-(2-naphthyl)alanine; Pic, pipecolic acid; Sar, sarcosine; HIV-1, human immunodeficiency virus type 1; RA, rheumatoid arthritis; SA-MD, simulated annealing molecular dynamics; AMD3100, 1,1′-[1,4-phenylenebis(methylene)]-bis(1,4,8,11-tetraazacyclotetradecane); KRH1636, *N*-{(*S*)-4-guanidino-1-[(*S*)-1-naphthalen-1-yl-ethylcarbamoyl]butyl}-4-{[(pyridin-2-yl-methyl)amino]methyl}benzamide.

10.1021/jm0607350 CCC: $37.00
Published on Web 12/29/2006

Scheme 1[a]

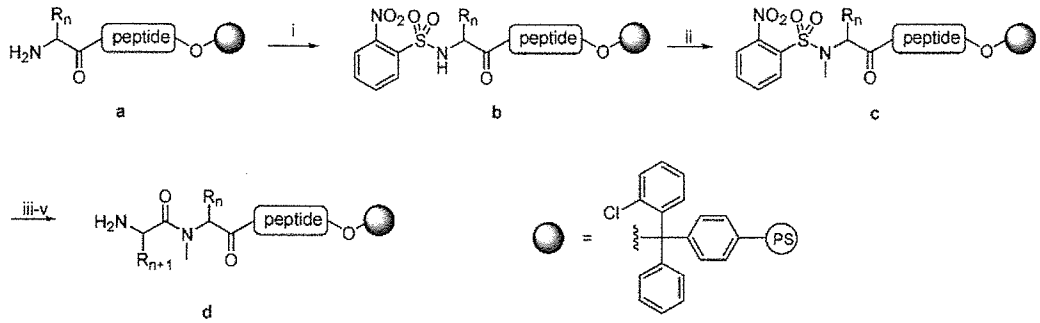

[a] Reagents: (i) *o*-nitrobenzenesulfonyl chloride, 2,4,6-collidine; (ii) MeOH, PPh_3, DEAD; (iii) DBU, 2-mercaptoethanol; (iv) Fmoc-AA-OH, HATU, HOAT, DIPEA; (v) piperidine.

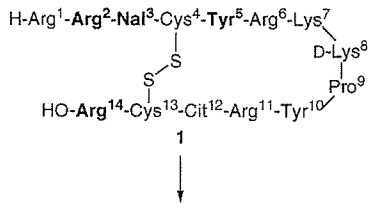

2 cyclo(-D-Tyr[1]-L-Arg[2]-L-Arg[3]-L-Nal[4]-L-Gly[5]-)

3 cyclo(-D-Tyr[1]-D-Arg[2]-L-Arg[3]-L-Nal[4]-L-Gly[5]-)

Figure 1. Structures of **1** and its downsized peptides **2** and **3**. Bold residues are the indispensable residues of **1** for the potent CXCR4-antagonistic activity. Nal = L-3-(2-naphthyl)alanine, Cit = L-citrulline.

correspond to the pharmacophore residues of the parent peptide **1**. We[25-27] and others[28] have performed several modifications on **2** including incorporation of (*E*)-alkene or reduced-amide dipeptide isosteres and conformationally constrained amino acid analogues, and fine-tuning of backbone ring structures. However, systematic modifications of **2** to design more potent antagonists have not been reported so far. In order to clarify the elements among the peptide side-chain and backbone functional groups indispensable for the ligand binding to CXCR4, chemical derivatization of **2** and **3** was conducted. In this manuscript, we describe the details of structure–activity relationship studies on cyclic pentapeptide-based CXCR4 antagonists **2** and **3** as well as identification of a more potent CXCR4 antagonist.

Chemistry. Synthesis on solid support of all peptides was performed on 2-chlorotrityl [(2-Cl)Trt] resin in parallel using usual Fmoc-based solid-phase peptide synthesis as described in the Experimental Section. *t*-Bu and 2,2,4,6,7-pentamethyldihydrobenzofuran-5-sulfonyl (Pbf) groups were employed for Tyr and Arg residue side-chain protection, respectively. L-Ala, D-Ala, L-Pro, D-Pro, L-pipecolic acid (L-Pic), D-Pic, β-alanine (β-Ala), and L-Nal were employed for the C-terminal residues of **12/19**, **13/20**, **14/21**, **15/22**, **16/23**, **17/24**, **18/25**, and **26/31**, respectively. The Gly residue was positioned at the C-terminal of the other peptide resins to avoid potential epimerization during the cyclization. For the preparation of *N*-methyl amino acid-containing peptide resins, an *N*-methyl group was incorporated on the α-amino group by a site-selective method reported by Miller et al.[29,30] (Scheme 1). The α-amino group was temporarily protected with an *o*-nitrobenzenesulfonyl (*o*-Ns) group before *N*-methylation by the Mitsunobu reaction. After removal of the *o*-Ns group by treatment with 1,8-diazabicyclo[5.4.0]undec-7-ene (DBU) and 2-mercaptoethanol, the subsequent amino acids were coupled using *O*-(7-azabenzotriazol-1-yl)-1,1,3,3-tetramethyluronium hexafluorophosphate (HATU)[31] as an activating reagent. Treatment of protected peptide resins with 20% (v/v) 1,1,1,3,3,3-hexafluoroisopropanol (HFIP) in CH_2Cl_2[32] provided linear protected peptides, which were cyclized with diphenylphosphoryl azide (DPPA) in DMF. Final deprotection with TFA–H_2O (95:5) followed by reverse-phase HPLC purification afforded the cyclic peptides. All peptides were identified with ion-spray mass spectrometry, and the purity was more than 95% by analytical HPLC.

Table 1. Biological Activities of **2**, **3**, and the Ala-Substituted Derivatives

peptide	sequence[a]	IC_{50} (μM)[b]	EC_{50} (μM)[c]
2	cyclo(-D-Tyr-L-Arg-L-Arg-L-Nal-Gly-)	0.004	0.16
4	cyclo(-D-Ala-L-Arg-L-Arg-L-Nal-Gly-)	>1	115
5	cyclo(-D-Tyr-L-Ala-L-Arg-L-Nal-Gly-)	0.063	12
6	cyclo(-D-Tyr-L-Arg-L-Ala-L-Nal-Gly-)	>1	>120
7	cyclo(-D-Tyr-L-Arg-L-Arg-L-Ala-Gly-)	>1	>120
3	cyclo(-D-Tyr-D-Arg-L-Arg-L-Nal-Gly-)	0.008	0.39
8	cyclo(-D-Ala-D-Arg-L-Arg-L-Nal-Gly-)	0.13	29
9	cyclo(-D-Tyr-D-Ala-L-Arg-L-Nal-Gly-)	0.23	16
10	cyclo(-D-Tyr-D-Arg-L-Ala-L-Nal-Gly-)	>1	60
11	cyclo(-D-Tyr-D-Arg-L-Arg-L-Ala-Gly-)	>1	>120

[a] The substituted residues from the parent peptides **2** and **3** are designated by underlining. [b] IC_{50} values for the cyclic pentapeptides are based on inhibition of [^{125}I]SDF-1 binding to CXCR4 transfectants of CHO cells. [c] EC_{50} values are based on the inhibition of HIV-induced cytopathogenicity in MT-4 cells. All data are the mean values for at least three independent experiments.

Results and Discussion

Identification of Indispensable Pharmacophore Functionality by Alanine-Scanning. Our first attempt was to identify the minimal side-chain functional group requirement of **2** and **3** for CXCR4 antagonism. To evaluate the comparative significance of side-chain functionality, each residue except for the Gly residue of **2** and **3** was substituted with Ala. Because the chirality of Ala was identical to that of the corresponding residue in parent peptides, exhibition of similar conformations was expected even after the substitution. All Ala-substituted peptides **4**–**11** showed significantly less CXCR4 antagonistic and anti-HIV activities when compared to the parent peptides **2** and **3**. Ala[3]- or Ala[4]-substituted analogues **6**, **7**, **10**, and **11** did not show any CXCR4 antagonistic activity up to 1 μM (Table 1). This indicates that all the side-chain functional groups are important for the high CXCR4 antagonistic activity. On the other hand, L/D-Ala[2]-substituted analogues, **5** and **9**, and D-Ala[1]-substituted analogue **8** maintained moderate activities (**5**: IC_{50} = 63 nM, EC_{50} = 12 μM; **8**: IC_{50} = 130 nM, EC_{50} = 29 μM; **9**: IC_{50} = 230 nM, EC_{50} = 16 μM), although the potencies were less than one-twentieth of the parent peptides. These data suggest that the phenol group of D-Tyr[1] and a guanidino group of Arg[2] do not play a critical role in receptor binding, while guanidino group of Arg[3] and naphthalene group of Nal[4] are indispensable for the ligand interaction with CXCR4. This

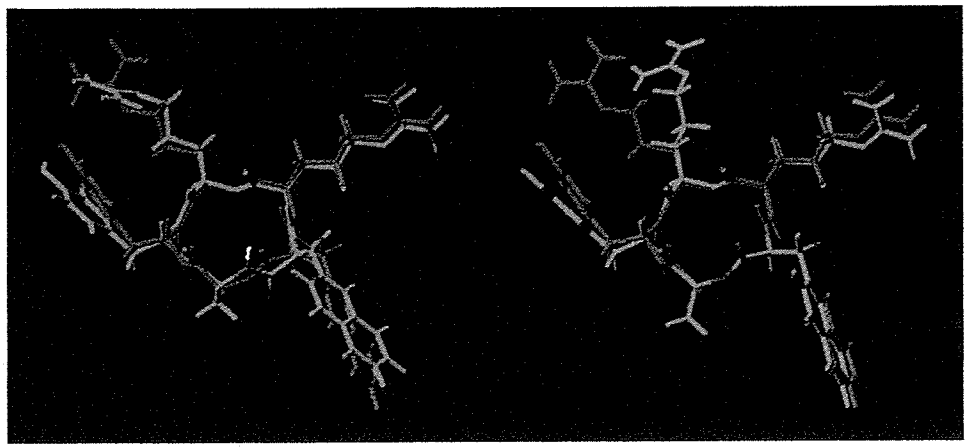

Figure 2. Superimposition of low-energy structures of **2** (purple) and **12** (green, left) or **13** (green, right).

propensity is consistent with the previous structure−activity relationship studies on **1**, where Ala-substitutions at the Arg^2-Nal^3 motif in **1** were more sensitive to anti-HIV activity as compared to the substitution of the other important residues, such as Tyr^5 and Arg^{14}.[24] It is noteworthy that two L/D-Ala^2-substituted peptides **5** and **9** having opposite chiralities retained moderate bioactivities. Recently, we have shown that L-Arg^2 in **2** could be replaced by nonbasic amino acids such as L-Phe-(4-F) (L-4-fluorophenylalanine) and D-MeAla without significant loss of CXCR4 antagonistic activity.[26,27] Hence, the functional group or the spatial disposition of the Arg^2 guanidino group could be further optimized.

Conformational Restriction of Cyclic Peptides by Modification of the Glycine Residue. In contrast to the finding that all side-chain functional groups of **2** and **3** were important for the high CXCR4 antagonistic activities, the Gly^5 position had many possibilities for further optimization. Since the absence of a side chain in Gly^5 possibly affected the conformational flexibility of the peptide backbone, it was expected that use of chiral or conformationally constrained amino acids would potentially restrict the global conformations to decrease the entropy losses upon the peptide binding on CXCR4. In order to evaluate the structure−activity relationship at the Gly^5 position, simple aliphatic amino acids were utilized for this study. In our previous conformational studies on **2**, characteristic orientations of the amide carbonyl groups of D-Tyr^1, Arg^2, Arg^3, and Gly^5 were observed in the low energy state.[23] These carbonyl oxygens were oriented away from the side chains of the respective following amino acids. This could be attributed to steric repulsion by a 1,3-allylic strain-like effect across the planar peptide bond.[33] On the other hand, the flexible Nal^4 ψ and Gly^5 ϕ angles had been expected, since there were two possibilities of Nal^4 carbonyl oxygen orientation. However, the carbonyl oxygen was directed away from the Gly^5 pro-*R* hydrogen atom in the calculated conformations, while the other orientation was not exhibited. This implied that the incorporation of a side chain having *R*-chirality (D-amino acid) at the Gly^5 position could restrict the rotation of the Nal^4-Gly^5 peptide bond plane. On the basis of this hypothesis, we introduced both enantiomers of Ala, Pro, and Pic to the Gly^5 position for conformational restriction. In addition, β-Ala was utilized for the optimization of carbon chain length at the Gly^5 position.

L-Ala^5-substituted analogues **12** and **19** showed less than 10-fold lower CXCR4 antagonistic and anti-HIV activities of the parent peptides **2** and **3**, respectively (Table 2, **12**: IC_{50} = 170 nM; EC_{50} = 20 μM, **19**: IC_{50} = 92 nM; EC_{50} = 10 μM). By contrast and as expected, more than 8-fold higher potencies were observed for D-Ala^5-substituted analogues **13** and **20** (**13**: IC_{50} = 11 nM; EC_{50} = 0.49 μM, **20**: IC_{50} = 11 nM; EC_{50} = 0.67 μM) as compared to the corresponding L-Ala^5-substituted peptides **12** and **19**, respectively. The bioactivities of D-Ala^5-substituted analogues were approximately half of the parent peptides **2** and **3**. This suggested that substitution with L-Ala^5 resulted in significant conformational change, while D-Ala^5 substitution kept the bioactive conformations of the parent peptides **2** and **3**. Simulated annealing molecular dynamics (SA-MD) analysis demonstrated that the backbone conformation of **13** was similar to that of **2** but different from that of **12** (Figure 2). Local conformations around Nal^4 and Gly^5/D-Ala^5 were very similar between **2** and **13** as expected, while the conformation of L-Ala^5-substituted analogues **12** differed particularly in the opposite orientation of the Nal^4 carbonyl oxygen. These calculated structures are consistent with the observed NOE data; in L-Ala^5-substituted peptide **13**, strong NOE between Nal^4 H^α and D-Ala^5 H^N indicates that these hydrogen atoms were oriented into the same direction. On the other hand, the observed weak NOE between Nal^4 H^α and L-Ala^5 H^N in peptide **12** indicates these hydrogen atoms were oriented into the opposite directions. The 1,3-pseudo allylic strain between the Nal^4 carbonyl oxygen and the α-methyl group of D/L-Ala^5 could result in these different conformational preferences between **12** and **13**. This

Table 2. Biological Activities of the Gly^5-Modified Analogues of **2** and **3**

peptide	sequence[a]	IC_{50} (μM)[b]	EC_{50} (μM)[c]
2	cyclo(-D-Tyr-L-Arg-L-Arg-L-Nal-Gly-)	0.004	0.16
12	cyclo(-D-Tyr-L-Arg-L-Arg-L-Nal-L-Ala-)	0.17	20
13	cyclo(-D-Tyr-L-Arg-L-Arg-L-Nal-D-Ala-)	0.011	0.49
14	cyclo(-D-Tyr-L-Arg-L-Arg-L-Nal-L-Pro-)	>1	-[d]
15	cyclo(-D-Tyr-L-Arg-L-Arg-L-Nal-D-Pro-)	>1	-[d]
16	cyclo(-D-Tyr-L-Arg-L-Arg-L-Nal-L-Pic-)	>1	-[d]
17	cyclo(-D-Tyr-L-Arg-L-Arg-L-Nal-D-Pic-)	>1	-[d]
18	cyclo(-D-Tyr-L-Arg-L-Arg-L-Nal-β-Ala-)	0.047	3.0
3	cyclo(-D-Tyr-D-Arg-L-Arg-L-Nal-Gly-)	0.008	0.37
19	cyclo(-D-Tyr-D-Arg-L-Arg-L-Nal-L-Ala-)	0.092	10
20	cyclo(-D-Tyr-D-Arg-L-Arg-L-Nal-D-Ala-)	0.011	0.67
21	cyclo(-D-Tyr-D-Arg-L-Arg-L-Nal-L-Pro-)	> 1	-[d]
22	cyclo(-D-Tyr-D-Arg-L-Arg-L-Nal-D-Pro-)	> 1	-[d]
23	cyclo(-D-Tyr-D-Arg-L-Arg-L-Nal-L-Pic-)	0.64	-[d]
24	cyclo(-D-Tyr-D-Arg-L-Arg-L-Nal-D-Pic-)	> 1	-[d]
25	cyclo(-D-Tyr-D-Arg-L-Arg-L-Nal-β-Ala-)	0.35	38

[a] The substituted residues from the parent peptide **2** and **3** are underlined. [b] IC_{50} values for the cyclic pentapeptides are based on inhibition of [^{125}I]SDF-1 binding to CXCR4 transfectants of CHO cells. [c] EC_{50} values are based on the inhibition of HIV-induced cytopathogenicity in MT-4 cells. [d] Not tested. All data are the mean values for at least three independent experiments.

Table 3. Biological Activities of *N*-Methyl Amino Acid-Containing Analogues of **2** and **3**

peptide	sequence[a]	IC_{50} (μM)[b]	EC_{50} (μM)[c]
2	cyclo(-D-Tyr-L-Arg-L-Arg-L-Nal-Gly-)	0.004	0.16
26	cyclo(-D-MeTyr-L-Arg-L-Arg-L-Nal-Gly-)	0.128	-[d]
27	cyclo(-D-Tyr-L-MeArg-L-Arg-L-Nal-Gly-)	0.023	1.399
28	cyclo(-D-Tyr-L-Arg-L-MeArg-L-Nal-Gly-)	0.099	9.534
29	cyclo(-D-Tyr-L-Arg-L-Arg-L-MeNal-Gly-)	0.250	-[d]
30	cyclo(-D-Tyr-L-Arg-L-Arg-L-Ala-Sar-)	0.167	-[d]
3	cyclo(-D-Tyr-D-Arg-L-Arg-L-Nal-Gly-)	0.008	0.39
31	cyclo(-D-MeTyr-D-Arg-L-Arg-L-Nal-Gly-)	0.157	-[d]
32	cyclo(-D-Tyr-D-MeArg-L-Arg-L-Nal-Gly-)	0.003	0.088
33	cyclo(-D-Tyr-D-Arg-L-MeArg-L-Nal-Gly-)	0.021	0.782
34	cyclo(-D-Tyr-D-Arg-L-Arg-L-MeNal-Gly-)	0.563	-[d]
35	cyclo(-D-Tyr-D-Arg-L-Arg-L-Nal-Sar-)	0.256	-[d]

[a] *N*-Methylated residues are underlined. [b] IC_{50} values for the cyclic pentapeptides are based on inhibition of [^{125}I]SDF-1 binding to CXCR4 transfectants of CHO cells. [c] EC_{50} values are based on the inhibition of HIV-induced cytopathogenicity in MT-4 cells. [d] Not tested. All data are the mean values for at least three independent experiments.

could explain the reason for the higher potencies of D-Ala^5-substituted analogues. The above information could serve for the further optimization of the Gly^5 position using D-amino acids having side-chain functionality.

Our next approach was to restrict global conformations of peptides **2** and **3** using cyclic amino acids such as L/D-Pro and L/D-Pic. These amino acids can provide a fused ring structure of cyclic peptides consisting of small and large rings. It was expected that the limited ϕ angle flexibility of Pro and Pic could contribute to the global conformational restriction.[34] Covalent linkage between the amide nitrogen and the side chain could also produce a favorable orientation of the Nal^4 carbonyl oxygen. However, L/D-Pro^5- and L/D-Pic^5-substituted peptides **14**−**17**, **21**, **22**, and **24** did not show CXCR4 inhibitory activities with IC_{50} values lower than 1 μM. Even the most potent peptide **23** exhibited an IC_{50} of only 0.64 μM. This suggests that the presence of cyclic amino acids at this position is sterically or conformationally unfavorable for the peptide−CXCR4 interaction. We could also assume that an amide proton at this position is required for high activity. This was supported by the fact that peptides having a sarcosin (Sar) at the Gly^5 position possessed less than one-thirtieth CXCR4 antagonistic activity of the parent peptides (see the next section). β-Ala^5-substituted analogues **18** and **25** showed lower CXCR4 antagonistic and anti-HIV activities (**18**: IC_{50} = 47 nM, EC_{50} = 3 μM; **25**: IC_{50} = 350 nM, EC_{50} = 38 μM), indicating that expansion of the backbone ring size (16-membered ring) at this position is not favorable. Recently, we showed that reduction in the size of the backbone ring using γ-Nal [4-amino-5-(2-naphthyl)pentanoic acid] or γ-(*E*)-Nal [(*E*)-4-amino-5-(2-naphthyl)pent-2-enoic acid] unit (14-membered ring) instead of Nal^4-Gly^5 dipeptide resulted in moderate to significant loss of CXCR4 antagonistic activity.[27] These observations suggest the importance of Gly^5 as a spacer for appropriate spatial orientation of the CXCR4 antagonist pharmacophores.

Identification of a Novel Potent CXCR4 Antagonist through *N*-Methyl Amino Acid-Scanning of 2 and 3. *N*-Methylation of the peptide backbone has been shown to be a valuable method in structure−activity relationship studies on bioactive peptides.[35−37] Substitutions with *N*-methyl amino acids often cause an increase or decrease in potency and selectivity of peptide ligands, providing useful information on the bioactive conformation. Hence, every amide bond of **2** and **3** was replaced sequentially with the corresponding *N*-methylated amide, and the bioactivities of obtained peptides were evaluated (Table 3).

Peptides **26**, **28**, **29**, and **30** derived from *N*-methyl amino acid-scanning of peptide **2** showed more than 25-fold less CXCR4 antagonistic activity as compared to the parent peptide **2**. *N*-Methylated analogues **31**, **34**, and **35** also showed a significant decrease in CXCR4 antagonism as compared to the parent peptide **3**. Use of L-MeArg^3 in peptide **33** slightly decreased the activity. *N*-Methylation at the Nal^4 position caused a remarkable decrease in CXCR4 antagonistic activity (**29**: IC_{50} = 250 nM; **34**: IC_{50} = 563 nM), suggesting that *N*-methylation at the putative receptor-binding motif (Arg^3-Nal^4) is unfavorable probably due to the absence of an amide proton. Previously, we showed that replacement of the Arg^3-Nal^4 motif with the corresponding (*E*)-alkene dipeptide isostere unit (L-Arg^3-ψ[(*E*)-CH=CH]-L-Nal^4) or a reduced amide isostere unit (L-Arg^3-ψ-[CH_2−NH]-L-Nal^4) caused a significant loss of CXCR4 antagonistic activity.[25] These observations also indicate the importance of the Arg^3-Nal^4 amide bond in both functional and conformational aspects.

On the other hand, the L/D-MeArg^2-substituded peptides **27** and **32** showed potent CXCR4 antagonistic and anti-HIV activities (**27**: IC_{50} = 23 nM, EC_{50} = 1.4 μM; **32**: IC_{50} = 3.0 nM, EC_{50} = 0.088 μM), indicating that *N*-methylation at Arg^2 is not critical to antagonist activity. Interestingly, the D-MeArg^2 substitution (**32**) led to approximately 2-fold increase of CXCR4 antagonistic activity and more than 40-fold anti-HIV activity as compared with **3**, and these activities were nearly equal to those of **2**. NMR and SA-MD calculations showed that major conformer of **32** exhibited a backbone conformation similar to **2** but different from the parent peptide **3**, particularly with respect to the orientation of D-Tyr^1 carbonyl oxygen (Figure 3).[38] This conformation was also supported by strong NOEs between [D-Arg^2 H$^\alpha$ and D-Arg^2 H^{NMe}] and [D-Arg^2 H^{NMe} and Arg^3 H^N] in **32** (the corresponding strong NOEs were not observed in the parent peptide **3**; see Supporting Information). It is possible that an unfavorable 1,3-pseudo-allylic strain-like effect between the *N*-methyl group of D-MeArg^2 and D-Tyr^1 side chain of **32** induced the flip of D-Tyr^1-D-Arg^2 amide group upon *N*-methylation of D-Arg^2, resulting in the identical local conformation around the D-Tyr^1-D-MeArg^2 dipeptide with the D-Tyr^1-L-Arg^2 conformation of **2**. Previously, we have shown a similar local conformational change upon *N*-methylation at the same position in D-Ala^2-substituted analogues of **2**; i.e. cyclo(-D-Tyr^1-D-MeAla^2-Arg^3-Nal^4-Gly^5-) showed 5-fold higher CXCR4 antagonistic activity (IC_{50} = 42 nM) than the nonmethylated peptide, cyclo(-D-Tyr^1-D-Ala^2-Arg^3-Nal^4-Gly^5-) **9**.[27] It is also noted that the lower bioactivities of peptide **27** compared to **2** could be explained by the potential flip of the D-Tyr^1-L-MeArg^2 amide bond orientation by *N*-methylation. These data suggest that the amide proton of Arg^2 has little contribution to bioactivity, and the amide bond orientation between D-Tyr^1 and D-MeArg^2 in **32** may contribute to its enhanced biological function.

Conclusion

Our present Ala-scanning study has shown that all of the side-chain functional groups contribute to high CXCR4 antagonistic activity of peptides **2** and **3**. In particular, Arg^3 and Nal^4 were proven to be indispensable for CXCR4 antagonistic activity. We have also shown that L-Ala substitution for Gly^5 of **2** or **3** caused a remarkable decrease in CXCR4 antagonistic and anti-HIV activities, while D-Ala substitution retained activity. Conformational studies revealed that D-Ala-substituted analogue **13** adopted a backbone conformation similar to that of **2**, which allows the rationalization of the biological activity for these

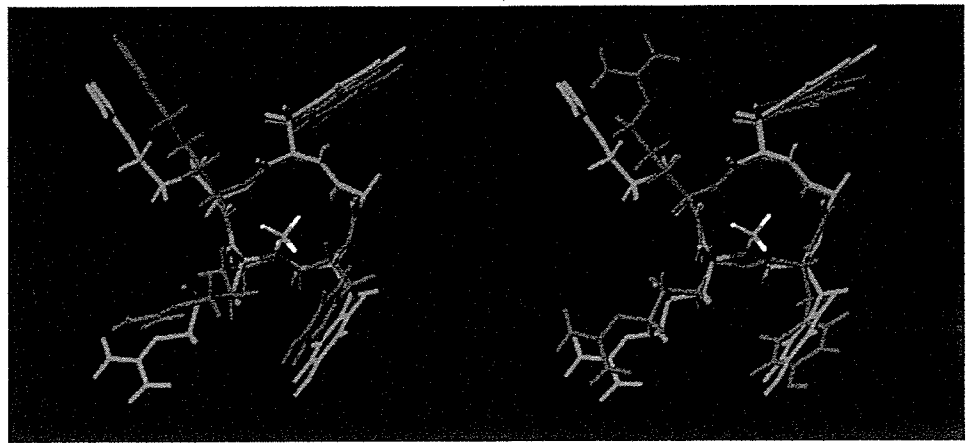

Figure 3. Superimposition of low-energy structures of **32** (green) and **2** (purple, left) or **3** (purple, right).

series of analogues. In addition, through comprehensive *N*-methyl-scanning of all residues in **2** and **3**, the *N*-methylated analogue **32** was characterized as one of the most potent cyclic pentapeptide-based CXCR4 antagonists synthesized thus far. The slight increase in CXCR4 antagonistic activity in **32** as compared to its nonmethylated analogue **3** could be explained by the favorable peptide bond orientation at the *N*-methylation site. Conformational studies suggested that the high potency in these series of compounds is due to the orientation of the backbone amide bonds, although direct interaction of the amide functions with the CXCR4 receptor is not clear. These results give valuable insight for understanding the ligand−receptor interactions and may also provide useful approaches for the design of new low-molecular-weight CXCR4 antagonists.

Experimental Section

General. Exact mass (HRMS) spectra were recorded on a JEOL JMS-01SG-2 or JMS-HX/HX 110A mass spectrometer. The ion-spray mass spectrum was obtained with a Sciex API*III*E triple quadrupole mass spectrometer (Toronto, Canada). Optical rotations were measured in water or 50% (v/v) water/AcOH solution with a Horiba high-sensitive polarimeter SEPA-200. ^{1}H NMR spectra were recorded using a Bruker AM 600 or JEOL JNM-ECA600 spectrometer at 600 MHz frequency, or JEOL JNM-AL400 spectrometer at 400 MHz frequency. Chemical shifts are calibrated to the solvent signal (2.49 ppm for DMSO, or 4.65 ppm for H_2O; s = singlet, d = doublet, dd = double doublet, m = multiplet). For HPLC separations, a Cosmosil 5C18-ARII analytical column (Nacalai Tesque, 4.6 × 250 mm, flow rate 1 mL/min) or a Cosmosil 5C18-ARII preparative column (Nacalai Tesque, 20 × 250 mm, flow rate 11 mL/min) was employed, and eluting products were detected by UV at 220 nm. A solvent system consisting of 0.1% TFA in water (v/v, solvent A) and 0.1% TFA in MeCN (v/v, solvent B) was used for HPLC elution.

Preparation of Amino Acid-Loaded 2-Chlorotrityl Resin. 2-Chlorotrityl chloride resin (1.25 mmol/g, 0.63 mmol) was treated with Fmoc-amino acid (0.69 mmol) and *N,N*-diisopropylethylamine (DIPEA) (2.77 mmol) in CH_2Cl_2 (5.00 mL) for 1.5 h. After the resin was washed with CH_2Cl_2, it was dried in vacuo. The loading was determined by measuring at 290 nm UV absorption of the piperidine-treated sample: Fmoc-L-Nal-(2-Cl)Trt-resin (0.72 mmol/g); Fmoc-L-Pro-(2-Cl)Trt-resin (0.78 mmol/g); Fmoc-D-Pro-(2-Cl)-Trt-resin (0.81 mmol/g); Fmoc-L-Pic-(2-Cl)Trt-resin (0.88 mmol/g); Fmoc-D-Pic-(2-Cl)Trt-resin (0.84 mmol/g); Fmoc-β-Ala-(2-Cl)Trt-resin (0.79 mmol/g).

Fmoc-Based Solid-Phase Peptide Synthesis. Protected peptide resins were manually constructed on a 0.10 mmol scale on H-L-Ala-(2-Cl)Trt-resin (0.89 mmol/g) for **12** and **19**, H-D-Ala-(2-Cl)-Trt-resin (0.90 mmol/g) for **13** and **20**, Fmoc-L-Pro-(2-Cl)Trt-resin for **14** and **21**, Fmoc-D-Pro-(2-Cl)Trt-resin for **15** and **22**, Fmoc-L-Pic-(2-Cl)Trt-resin for **16** and **23**, Fmoc-D-Pic-(2-Cl)Trt-resin for **17** and **24**, Fmoc-β-Ala-(2-Cl)Trt-resin for **18** and **25**, Fmoc-L-Nal-(2-Cl)Trt-resin for **26** and **31**, and H-Gly-Trt(2-Cl)Trt-resin (0.75 mmol/g) for the other peptides. Fmoc-amino acids were coupled using 1,3-diisopropylcarbodiimide (DIPCDI, 0.078 mL, 0.50 mmol) and *N*-hydroxybenzotriazole hydrate (HOBt·H_2O, 76 mg, 0.50 mmol) in DMF (1.0 mL) for 1.5 h. For the coupling of Fmoc-amino acid to the *N*-methyl amino acid, HATU (186 mg, 0.49 mmol) and 1-hydroxy-7-azabenzotriazole (HOAt, 68 mg, 0.50 mmol) were employed in place of DIPCDI/HOBt. The Fmoc group was deprotected by treatment with 20% (v/v) piperidine−DMF for 20 min.

***N*-Methyl Modification of *N*-Terminal α-Amino Group on Resin.** Resin (0.10 mmol) was treated with *o*-nitrobenzenesulfonyl chloride (66.5 mg, 0.30 mmol) and 2,4,6-collidine (0.066 mL, 0.50 mmol) in CH_2Cl_2 (1.0 mL) for 2 h at room temperature. After the resin was washed (CH_2Cl_2 × 3, DMF × 3, and THF × 3), to a suspension of the *N*-Ns-protected resin in anhydrous THF (1.0 mL) were added MeOH (0.020 mL, 0.50 mmol), PPh_3 (131 mg, 0.50 mmol), and diethyl diazodicarboxylate (0.227 mL, 0.50 mmol) at 0 °C. The mixture was shaken for 2 h at room temperature, followed by washing the resin (THF × 3 and $CHCl_3$ × 3). The *N*-methylated resin was treated with DBU (0.075 mL, 0.50 mmol) and 2-mercaptoethanol (0.070 mL, 1.0 mmol) for 1.5 h at room temperature to give the protected peptide resin having an *N*-methyl amino acid at the *N*-terminus.

Cleavage of Protected Peptides from the Resin and Cyclization. Protected peptide resin was treated with 20% (v/v) HFIP−CH_2Cl_2 (10 mL) for 2 h. After filtration of the resin, the filtrate was concentrated to provide the crude linear protected peptide. To the solution of the residue in DMF (30 mL) were added DPPA (0.539 mL, 0.25 mmol) and $NaHCO_3$ (42.0 mg, 0.50 mmol) at −40 °C. After being stirred for 36 h at room temperature, the whole was filtered, and the filtrate was concentrated to give the protected cyclic peptide, which was subjected to solid-phase extraction (SPE) over basic alumina in $CHCl_3$−MeOH (9:1) to remove inorganic salts derived from DPPA.

Deprotection of Protected Cyclic Peptide and HPLC purification. Protected cyclic peptides were treated with 95% (v/v) TFA solution (10 mL) for 2 h at room temperature. Concentration under reduced pressure and purification by preparative HPLC gave cyclic peptides.

Cell Culture. Human T-cell lines, MT-4 and MOLT-4 cells were grown in RPMI 1640 medium containing 10% heat-inactivated fetal calf serum, 100 IU/mL penicillin, and 100 μg/ mL streptomycin.

Virus. A strain of X4-HIV-1, HIV-1IIIB, was used for the anti-HIV assay. This virus was obtained from the culture supernatant of HIV-1 persistently infected MOLT-4/HIVIIIB cells and stored at −80 °C until used.

Anti-HIV-1 Assay. Anti-HIV-1 activity was determined based on the protection against HIV-1-induced cytopathogenicity in MT-4

cells. Various concentrations of test compounds were added to HIV-1 infected MT-4 cells at multiplicity of infection (MOI) of 0.01 and placed in wells of a flat-bottomed microtiter tray (1.5×10^4 cells/ well). After 5 days incubation at 37 °C in a CO_2 incubator, the number of viable cells was determined using the 3-(4,5-dimethylthiazol-2-yl)-2,5-diphenyltetrazolium bromide (MTT).

[^{125}I]-SDF-1 Binding and Displacement. Stable CHO cell transfectants expressing CXCR4 variant were prepared as describe previously.[39] CHO transfectants were harvested by treatment with trypsin−EDTA, allowed to recover in complete growth medium (MEM-α, 100 μg/ mL penicillin, 100 μg/mL streptomycin, 0.25 μg/mL amphotericin B, 10% (v/v)) for 4−5 h, and then washed in cold binding buffer (PBS containing 2 mg/mL BSA). For ligand binding, the cells were resuspended in binding buffer at 1×10^7 cell/mL, and 100 μL aliquots were incubated with 0.1 nM of [^{125}I]-SDF-1 (Perkin-Elmer Life Sciences) for 2 h on ice under constant agitation. Free and bound radioactivities were separated by centrifugation of the cells through an oil cushion, and bound radioactivity was measured with gamma-counter (Cobra, Packard, Downers Grove, IL). Inhibitory activity of test compounds was determined based on the inhibition of [^{125}I]-SDF-1 binding to CXCR4 transfectants (IC_{50}).

NMR Spectroscopy. The peptide sample was dissolved in DMSO-d_6 at a concentration of 5 mM. ^{1}H NMR spectra of the peptides were recorded at 300 K. The assignment of the proton resonance was achieved by use of ^{1}H−^{1}H COSY spectra. $^3J(H^N, H^\alpha)$ coupling constants were measured from one-dimensional spectra. The mixing time for NOESY experiments was set at 200 ms. NOESY spectra were composed of 512 real points in the F2 dimension and 256 real points, which were zero-filled to 256 points in the F1 dimension, with 144 scans per t1 increment. The cross-peak intensities were evaluated by relative build-up rates of the cross-peaks. **2**, **3**, **12**, and **13** exhibited one set of signals in ^{1}H NMR spectra. On the other hand, two distinct sets of signals were observed in ^{1}H NMR spectra of **32** with relative populations of 69% and 31%, indicating the existence of two conformations. For the minor conformer, NOESY spectra showed the NOE contact between α protons of D-Tyr^1 and D-MeArg^2 which is characteristic of the amide bond in a *cis* conformation. The major conformer did not exhibit any sequential H^α−H^α NOEs, suggesting this conformer adopt an all-*trans* conformation. The calculated structures of major and minor conformers exhibited *trans*- and *cis*-D-Tyr^1-D-MeArg^2 amide bond, respectively, which was consistent with the observed NOEs.

Calculation of Structures. The structure calculations were performed on a Silicon Graphics Origin 2000 workstation with the NMR refine program within the Insight II/Discover package using the consistent valence force field (CVFF). Pseudoatoms were defined for the CH_3^α protons of L-Ala^5 of **12**, D-Ala^5 of **13**, and *N*-methyl protons of **32**, and for all methylene protons of Nal^4, D-Tyr^1, D/L-Arg^2, and Arg^3, prochirality of which were not identified from ^{1}H NMR data. The dihedral ϕ angle constraints were calculated based on the Karplus equation: $^3J(H^N, H^\alpha) = 6.7 \cos^2(\theta - 60°) - 1.3 \cos(\theta - 60°) + 1.5$. Lower and upper angle errors were set to 15°. The NOESY spectrum with a mixing time of 200 ms was used for the estimation of the distances restraints between protons. The NOE intensities were classified into three categories (strong, medium, and weak) based on the number of contour lines in the cross-peaks to define the upper-limit distance restraints (1.7, 3.5, and 5.0 Å, respectively). The upper-limit restraints were increased by 1.0 Å for the involved pseudoatoms. Lower bounds between nonbonded atoms were set to their van der Waals radii (1.8 Å). These distance and dihedral angle restraints were included with force constants of 25−100 kcal/mol·Å^2 and 25−100 kcal/mol·rad^2, respectively. The 50 initial structures generated by the NMR refine program randomly were subjected to the simulated annealing calculations. The final minimization stage was achieved until the maximum derivative became less than 0.01 kcal/mol·Å^2 by the steepest descents and conjugate gradients methods. Excellent convergence was seen in the backbone structure of all calculated structures. The root-mean-square deviation (rmsd) values for all backbone structures of ten low-energy structures were below 0.23 Å.

Acknowledgment. This work was supported by Grant-in-Aid for Scientific Research from the Ministry of Education, Culture, Sports, Science, and Technology of Japan, and Health and Labour Sciences Research Grants (Research on HIV/AIDS) and Philip Morris USA Inc. and Philip Morris International. Computation time was provided by the Supercomputer Laboratory, Institute for Chemical Research, Kyoto University. S.U. and S.O. are grateful for the JSPS Research Fellowships for Young Scientists.

Supporting Information Available: Characterization data for all new compounds, ^{1}H NMR data of **2**, **3**, **12**, **13**, and **32**, and HPLC charts of representative compounds. This material is available free of charge via the Internet at http://pubs.acs.org.

References

(1) Murphy, P. M.; Baggiolini, M.; Charo I. F.; Herbert, C. A.; Horuk, R.; Matsushima, K.; Miller, L. H.; Oppenheim, J. J.; Power, C. A. International union of pharmacology. XXII. Nomenclature for chemokine receptors. *Pharmacol. Rev.* **2000**, *52*, 145−176.
(2) Mackay, C. R.; Chemokines: immunology's high impact factors. *Nat. Immunol.* **2001**, *2*, 95−101.
(3) Premack, B. A.; Schall, T. J. Chemokine receptors: gateways to inflammation and infection. *Nat. Med.* **1996**, *2*, 1174−1178.
(4) Zlotnik, K.; Yoshie, O. Chemokines: a new classification system and their role in immunity. *Immunity* **2000**, *12*, 121−127.
(5) Bleul, C. C.; Fuhlbrigge, R. C.; Casanovas, J. M.; Aiuti, A.; Springer, T. A. A highly efficacious lymphocyte chemoattractant, stromal cell-derived factor 1 (SDF-1). *J. Exp. Med.* **1996**, *2*, 1101−1109.
(6) Tachibana, K.; Hirota, S.; Iizasa, H.; Yoshida, H.; Kawabata, K.; Kataoka, Y.; Kitamura, Y.; Matsushima, K.; Yoshida, N.; Nishikawa, S.; Kishimoto, T.; Nagasawa, T. The chemokine receptor CXCR4 is essential for vascularization of the gastrointestinal tract. *Nature* **1998**, *393*, 591−594.
(7) Nagasawa, T.; Hirota, S.; Tachibana, K.; Takakura, N.; Nishikawa, S.; Kitamura, Y.; Yoshida, N.; Kikutani, H.; Kishimoto, T. Defects of B-cell limphopoiesis and bone-marrow myelopoiesis in mice lacking the CXC chemokine PBSF/SDF-1. *Nature* **1996**, *382*, 635−638.
(8) Aiuti, A.; Webb, I. J.; Bleul, C.; Springer, T.; Gutierrez-Ramos, J. C. The chemokine SDF-1 is a chemoattractant for human CD34$^+$ hematopoietic progenitor cells and provides a new mechanism to explain the mobilization of CD34$^+$ progenitors to peripheral blood. *J. Exp. Med.* **1997**, *2*, 111−120.
(9) Zhu, Y.; Yu, Y.; Zhang, X. C.; Nagasawa, T.; Wu, J. Y.; Rao, Y. Role of the chemokine SDF-1 as the meningeal attractant for embryonic cerebellar neurons. *Nat. Neurosci.* **2002**, *5*, 719−720.
(10) Stumm, R. K.; Zhou, C.; Ara, T.; Lazarini, F.; Dubois-Dalcq, M.; Nagasawa, T.; Hollt, V.; Schulz, S. CXCR4 regulates interneuron migration in the developing neocortex. *J. Neurosci.* **2003**, *23*, 5123−5130.
(11) Feng, Y.; Broder, C. C.; Kennedy, P. E.; Berger, E. A. HIV-1 entry co-factor: Functional cDNA cloning of a seven-transmembrane G protein-coupled receptor. *Science* **1996**, *272*, 872−877.
(12) Oberlin, E.; Amara, A.; Bachelerie, F.; Bessia, C.; Virelizier, J. L.; Arenzana-Seisdedos, F.; Schwartz, O.; Heard, J. M.; Clark-Lewis, I.; Legler, D. L.; Loetscher, M.; Baggiolini, M.; Moser, B. The CXC chemokine SDF-1 is the ligand for LESTR/fusin and prevents infection by T-cell-line-adapted HIV-1. *Nature* **1996**, *382*, 833−835.
(13) Müller, A.; Homey, B.; Soto, H.; Ge, N.; Catron, D.; Buchanan, M. E.; Mcclanahan, T.; Murphy, E.; Yuan, W.; Wagner, S. M.; Barrera, J. L.; Mohar, A.; Verástegui, E.; Zlotnik, A. Involvement of chemokine receptors in breast cancer metastasis. *Nature* **2001**, *410*, 50−56.
(14) Nanki, T.; Hayashida, K.; El-Gabalawy, H. S.; Suson, S.; Shi, K.; Girschick, H. J., Yavuz, S.; Lipsky, P. E. Stromal cell-derived factor-1-CXC chemokine receptor interactions play a central role in CD4$^+$ T cell accumulation in rheumatoid arthritis synovium. *J. Immunol.* **2000**, *165*, 6590−6598.
(15) Masuda, M.; Nakashima, H.; Ueda, T.; Naba, H.; Ikoma, R.; Otaka, A.; Terakawa, Y.; Tamamura, H.; Ibuka, T.; Murakami, T.; Koyanagi, Y.; Waki, M.; Matsumoto, A.; Yamamoto, N.; Funakoshi, S.; Fujii,

N. A novel anti-HIV synthetic peptide, T-22 ([Tyr^{5,12},Lys^{7}]-polyphemusin II). *Biochem. Biophys. Res. Commun.* **1992**, 189, 845−850.
(16) Tamamura, H.; Xu, Y.; Hattori, T.; Zhang, X.; Arakaki, R.; Kanbara, K.; Omagari, A.; Otaka, A.; Ibuka, T.; Yamamoto, N.; Nakashima, H.; Fujii, N. A low molecular weight inhibitor against the chemokine redeptor CXCR4: a strong anti-HIV peptide T140. *Biochem. Biophys. Res. Commun.* **1998**, *253*, 877−882.
(17) Tamamura, H.; Hori, A.; Kanzaki, N.; Hiramatsu, K.; Mizumoto, M.; Nakashima, H.; Yamamoto, N.; Otaka, A.; Fujii, N. T140 analogues as CXCR4 antagonists identified as anti-metastatic agent in the treatment of breast cancer. *FEBS Lett.* **2003**, *550*, 79−83.
(18) Takenaga, M.; Tamamura, H.; Hiramatsu, K.; Nakamura, N.; Yamaguchi, Y.; Kitagawa, A.; Kawai, S.; Nakashima, H.; Fujii, N.; Igarashi, R. A single treatment with microcapsules containing a CXCR4 antagonist suppressed pulmonary metastasis of murine melanoma. *Biochem. Biophys. Res. Commun.* **2004**, 320, 226−232.
(19) Tamamura, H.; Fujisawa, M.; Hiramatsu, K.; Mizumoto, M.; Nakashima, H.; Yamamoto, N.; Otaka, A.; Fujii, N. Identification of a CXCR4 antagonist, T140 analog, as anti-rheumatoid arthritis agent. *FEBS Lett.* **2004**, *569*, 99−104.
(20) Schols, D.; Struyf, S.; Van Damme, J.; Este, J. A,; Henson, G.; De Clarcq, E. Inhibition of T-tropic HIV strains by selective antagonization of the chemokine receptor CXCR4. *J. Exp. Med.* **1997**, *186*, 1383−1388.
(21) Donzella, G. A.; Schols, D.; Lin, S. W.; Este, J. A.; Nagashima, K. A.; Maddon P. J. AMD3100, a small molecule inhibitor of HIV-1 entry via the CXCR4 co-receptor. *Nat. Med.* **1998**, *4*, 72−76.
(22) Ichiya, K.; Yokoyama-Kumakura, S.; Tanaka, Y.; Tanaka, R.; Hirose, K.; Bannai, K.; Edamatsu, T.; Yanaka, M.; Niitani, Y.; Miyano-Kurosaki, N.; Takaku, H.; Koyanagi, Y.; Yamamoto, N. A duodenally absorbable CXC chemokine receptor 4 antagonist, KRH-1636, exhibits a potent and selective anti-HIV-1 activity. *Proc. Natl. Acad. Sci. U.S.A.* **2003**, *100*, 4185−4190.
(23) Fujii, N.; Oishi, S.; Hiramatsu, K.; Araki, T.; Ueda, S.; Tamamura, H.; Otaka, A.; Kusano, S.; Terakubo, S.; Nakashima, H.; Broach, J. A.; Trent, J. O.; Wang, Z.; Peiper, S. C. Molecular-size reduction of a potent CXCR4-chemokine antagonist using orthogonal combination of conformation- and sequence-based libraries. *Angew. Chem. Int. Ed.* **2003**, *42*, 3251−3253.
(24) Tamamura, H.; Omagari, A.; Oishi, S.; Kanamoto, T.; Yamamoto, N.; Peiper, S. C.; Nakashima, H.; Otaka, A.; Fujii, N. Pharmacophore identification of a specific CXCR4 inhibitor, T140, lead to development of effective anti-HIV agents with very high selectivity indexes. *Bioorg. Med. Chem. Lett.* **2000**, *10*, 2633−2637.
(25) Tamamura, H.; Hiramatsu, K.; Ueda, S.; Wang, Z.; Kusano, S.; Terakubo, S.; Trent, J. O.; Peiper, S. C.; Yamamoto, N.; Nakashima, H.; Otaka, A.; Fujii, N. Stereoselective synthesis of [L-Arg-L/ D-3-(2-naphthyl)alanine]-type (*E*)-alkene dipeptide isosteres and its application to the synthesis and biological evaluation of pseudopeptide analogues of the CXCR4 antagonist FC131. *J. Med. Chem.* **2005**, *48*, 380−391.
(26) Tamamura, H.; Esaka, A.; Ogawa, T.; Araki, T.; Ueda, S.; Wang, Z.; Trent, J. O.; Tsutsumi, H.; Masuno, H.; Nakashima, H.; Yamamoto, N.; Peiper, S. C.; Otaka, A.; Fujii, N. Structure-activity relationship studies on CXCR4 antagonists having cyclic pentapeptide scaffolds. *Org. Biomol. Chem.* **2005**, *3*, 4392−4394.
(27) Tamamura, H.; Araki, T.; Ueda, S.; Wang, Z.; Oishi, S.; Esaka, A.; Trent, J. O.; Nakashima, H.; Yamamoto, N.; Peiper, S. C.; Otaka, A.; Fujii, N. Identification of novel low molecular weight CXCR4 antagonists by structural tuning of cyclic tetrapeptide scaffolds. *J. Med. Chem.* **2005**, *48*, 3280−3289.
(28) Marshall, G. R.; Wu, Y.; Heyden, N. V.; Ratner, L.; Nikiforovich, G. V. Backbone modification of cyclic pentapeptide antagonist of CXCR4. In *Peptides 2004 (Proceedings of 3rd international and 28th European peptide symposium)*; Flegel, M., Fridkin, M., Gilon, C., Slaninova, J., Eds.; Kenes International: Switzerland, 2005; pp 748−749.
(29) Miller, S. C.; Scanlan, T. S. Site-selective N-methylation of peptides on solid support. *J. Am. Chem. Soc.* **1997**, *119*, 2301−2302.
(30) Lin, X.; Dorr, H.; Nuss, J. M. Utilization of Fukuyama's sulfonamide protecting group for the synthesis of *N*-substituted α-amino acids and derivatives. *Tetrahedron Lett.* **2000**, *41*, 3309−3313.
(31) Carpino, L. A.; 1-Hydroxy-7-azabenzotriazole. An efficient peptide coupling additive. *J. Am. Chem. Soc.* **1993**, *115*, 4397−4398.
(32) Bollhagen, R.; Schmiedberger, M.; Barlos. K.; Grell. E. A new reagent for the cleavage of fully protected peptides synthesised on 2-chlorotrityl chloride resin. *J. Chem. Soc., Chem. Commun.* **1994**, 2559−2560.
(33) Haubner, R.; Finsinger, D.; Kessler, H. Stereoisomeric peptide libraries and peptidomimetics for designing selective inhibitors of the $\alpha_v\beta_3$ integrin for a new cancer therapy. *Angew. Chem. Int. Ed. Engl.* **1997**, *36*, 1374−1389.
(34) Toniolo, C. Conformationally restricted peptides through short range cyclization. *Int. J. Pept. Protein Res.* **1990**, *35*, 287−300.
(35) Dechantsreiter, M. A.; Planker, Eckart.; Matha, B.; Lohof, E.; Hölzemann, G.; Jonczyk, A.; Goodman, S. L.; Kessler, H. *N*-Methylated cyclic RGD peptides as highly active and selective $\alpha_v\beta_3$ integrin antagonists. *J. Med. Chem.* **1998**, *42*, 3033−3040.
(36) Rajeswaran, W. G.; Hocart, S. J.; Murphy, W. A.; Taylor, J. E.; Coy, D. H. Highly potent and subtype selective ligand derived by *N*-methyl scan of a somatostatin antagonist. *J. Med. Chem.* **2001**, *44*, 1305−1311.
(37) Erchegyi, J.; Hoeger, C. A.; Low, W.; Hoyer, D.; Waser, B.; Eltschinger, V.; Schaer, J.; Cescato, R.; Reubi, J. C.; Rivier, J. E. Somatostatin receptor 1 selective analogues: 2. N^{α}-Methylated Scan. *J. Med. Chem.* **2005**, *48*, 507−514.
(38) **32** exhibited two sets of signals in ^{1}H NMR spectra. The signals were assigned to *trans*- (69%) and *cis*- (31%) conformers at D-Tyr^1-D-MeArg^2 amide bond. Since backbone conformation and side chain disposition of *cis*-conformer of **32** was apparently different from the parent peptides **2** and **3**, we assumed that the major *trans*-conformer could contribute to the bioactivities of **32**, although contribution of the minor *cis*-conformer cannot be ruled out.
(39) Navenot, J. M.; Wang, Z. X.; Trent, J. O.; Murray, J. L.; Hu, Q. X.; DeLeeuw, L.; Moore, P. S.; Chang, Y.; Peiper, S. C. Molecular anatomy of CCR5 engagement by physiologic and viral chemokines and HIV-1 envelope glycoproteins; Differences in primary structural requirements for RANTES, MIP-1α, and vMIP-II binding. *J. Mol. Biol.* **2001**, *59*, 380−393.

JM0607350

A novel one-pot reaction involving organocopper-mediated reduction/transmetalation/asymmetric alkylation, leading to the diastereoselective synthesis of functionalized (*Z*)-fluoroalkene dipeptide isosteres†

Tetsuo Narumi,[a] Ayumu Niida,[a] Kenji Tomita,[a] Shinya Oishi,[a] Akira Otaka,[ab] Hiroaki Ohno[a] and Nobutaka Fujii*[a]

Received (in Cambridge, UK) 16th June 2006, Accepted 14th September 2006
First published as an Advance Article on the web 28th September 2006
DOI: 10.1039/b608596b

By a novel one-pot reaction sequence involving consecutive organocopper-mediated reduction, transmetalation and asymmetric alkylation, a highly diastereoselective synthesis of functionalized (*Z*)-fluoroalkene dipeptide isosteres was achieved in good to excellent yields.

Alkene-based dipeptide isosteres containing (*E*)-alkene or (*Z*)-fluoroalkene units are thought to be potential dipeptide mimetics.[1,2] (*Z*)-Fluoroalkene dipeptide isosteres are structurally similar to (*E*)-alkene dipeptide isosteres (EADIs), but differ in their electrostatic nature, which plays a significant role in their intra- and intermolecular interactions. Of note, due to the presence of the highly electronegative fluorine substituent, (*Z*)-fluoroalkene dipeptide isosteres more faithfully resemble native peptides than do EADIs. In this regard, there is increasing interest in the development of efficient methodologies for the stereoselective and divergent synthesis of (*Z*)-fluoroalkene isosteres.

The organocopper- or samarium diiodide (SmI_2)-mediated reduction of α,β-enoates, possessing leaving group(s) at the γ-position, is an effective methodology for the stereoselective synthesis of (*E*)-olefins and (*Z*)-fluoroolefins.[3,4] The dienolate intermediates resulting from the reduction can be efficiently trapped *in situ* by an appropriate electrophile, such as alkyl halides, aldehydes and ketones. Recently, we have applied this reduction/direct alkylation methodology to the synthesis of α-alkylated (*E*)-alkene and (*Z*)-fluoroalkene dipeptide isosteres (Fig. 1).[5,6] Although this reduction/direct alkylation of the difluoroenoate **1** is extremely useful for the regio- and stereoselective formation of the required (*Z*)-fluoroalkene unit, this synthetic route has not addressed the stereoselective construction of α-side chains. Since amino acids have a center of chirality, the equivalent side chains must be introduced with high stereoselectivity into the peptide isosteres. Herein, we report the diastereoselective synthesis of highly functionalized (*Z*)-fluoroalkene dipeptide isosteres by a novel one-pot reaction sequence, involving organocopper-mediated reduction, transmetalation and asymmetric alkylation as the key steps.

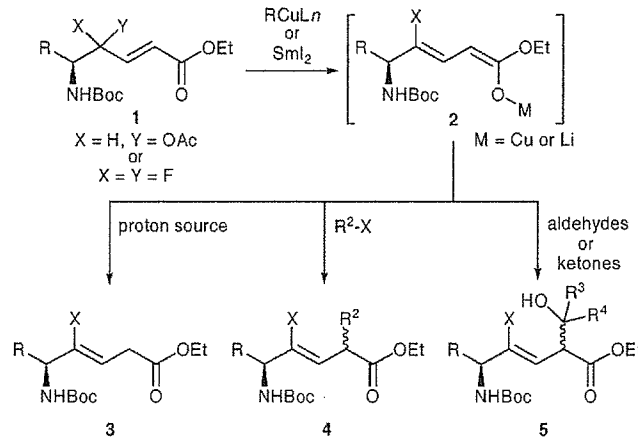

Fig. 1 Synthesis of (*E*)-alkene or (*Z*)-fluoroalkene dipeptide isosteres by a reduction/direct alkylation methodology.

The synthesis of the key intermediates, *N*-enoyl sultams **8** and **9**, is illustrated in Scheme 1. The α,α-difluoro-β-amino ester **7**[6] was reduced to an aldehyde and then subjected to Horner–Wadsworth–Emmons-type coupling with (*S*)- or (*R*)-*N*-diethoxyphosphonoacetylcamphorsultam[7] to give *N*-enoyl sultam **8** or **9** in an *E*-selective manner.

Initially, we examined the organocopper- and SmI_2-mediated reduction of **8**. Both reactions, using the Gilman reagent ($Me_2CuLi{\cdot}LiI{\cdot}2LiBr$ at −78 °C for 30 min) and the cyano

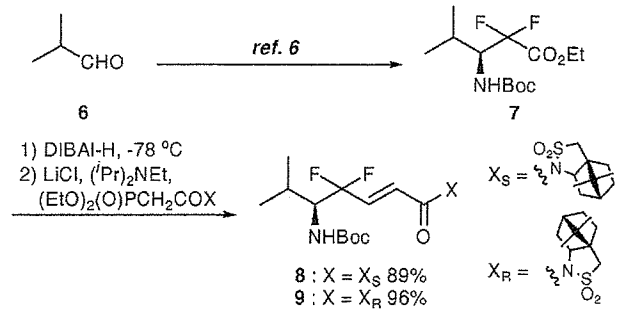

Scheme 1 Synthesis of the substrate for one-pot organocopper-mediated reduction/asymmetric alkylation.

[a]*Graduate School of Pharmaceutical Sciences, Kyoto University, Sakyo-ku, Kyoto 606-8501, Japan. E-mail: nfujii@pharm.kyoto-u.ac.jp*
[b]*Graduate School of Pharmaceutical Sciences, The University of Tokushima, Tokushima 770-8505, Japan*

† Electronic supplementary information (ESI) available: Experimental procedures, spectral data and analytical data for **12a**, and copies of ^1H and ^{13}C NMR spectra for all new compounds. See DOI: 10.1039/b608596b

Gilman reagent ($Me_2CuLi{\cdot}LiCN{\cdot}2LiBr$ at −78 °C for 30 min), proceeded smoothly to yield the desired reduction product in 95 and 74% yields, respectively (Table 1, entries 1 and 2). Although the electron-donating ability of higher order cuprate ($Me_3CuLi_2{\cdot}LiI{\cdot}3LiBr$) is more effective than those of the Gilman and cyano Gilman reagents,[8] the reaction of **8** with higher order cuprate ($Me_3CuLi_2{\cdot}LiI{\cdot}3LiBr$ at −78 °C for 30 min) afforded the reduction product in only a moderate yield (Table 1, entry 3). On the other hand, reaction with SmI_2,[9] which is well-recognized as a powerful one-electron reducing reagent,[10] afforded only a mixture of unidentified compounds (Table 1, entry 4). Based on these results, we chose the Gilman reagent as our reducing reagent.

Next, we carefully examined trapping of the dienolate intermediate with alkyl halides to construct the stereogenic center at the α-position. Initial attempts to trap the Cu or Li dienolates of intermediate **11a**, derived from **8** by organocopper-mediated reduction, with methyl iodide only furnished complex mixtures (Scheme 2). This prompted us to use the more reactive tin dienolate, which could be generated by the organocopper-mediated reduction of **8**, followed by treatment with triphenyltin chloride and HMPA.[11] Sequential reaction of **8** with Gilman reagent, triphenyltin chloride/HMPA and methyl iodide selectively afforded the α-methyl fluoroalkene isostere derivative (L-Val–ψ[(*Z*)-CF=CH]–L-Ala) (**12a**) in 93% isolated yield with exclusive *Z*-selectivity.‡ The diastereoselectivity of this reaction proved to be 80%, which was confirmed by RP-HPLC analysis.

In a similar manner, the use of benzyl bromide, *tert*-butyl bromoacetate and allyl bromide stereoselectively gave the corresponding α-substituted fluoroalkene dipeptide isosteres **12b**, **12c** and **12d**, respectively, in excellent yields (Table 2, entries 2 to 4). The reaction with methyl 3-bromopropionate gave the reduction product **10** with no alkylated product (Table 2, entry 5). Next, we attempted to synthesize epimeric (L,D)-type isosteres in a similar manner using (*R*)-sultam derivatives **9**. The reaction with Gilman reagent, followed by asymmetric alkylation *via* transmetalation, proceeded smoothly to afford the corresponding (L,D)-type α-substituted fluoroalkene isosteres **13a–13d** in high yields and with good to excellent diastereoselectivities (Table 2, entries 6 to 9).

Finally, the chiral auxiliary of **12b** was removed by hydrolysis under basic conditions to give the Boc–L-Val–ψ[(*Z*)-CF=CH]–L-Phe–OH isostere (**14**) in 75% yield with 96% de (Scheme 3). We observed neither epimerization of the α-alkyl groups nor isomerization of the double bond during cleavage of the chiral auxiliary.§

In conclusion, we have developed a novel and highly diastereoselective one-pot synthesis of functionalized (*Z*)-fluoroalkene dipeptide isosteres. The utility of the newly developed methodology can be found in the high-to-excellent regio- and stereoselectivities upon construction of the (*Z*)-fluoroalkene unit and α-side chain. Further studies using the developed methodology on the synthesis and evaluation of bioactive peptides with fluoroalkene isosteres are now in progress.

Table 1 Organocopper- and SmI_2-mediated reduction of *N*-enoyl sultam **8**

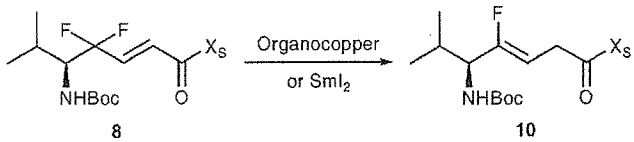

8 **10**

Entry	Reagent (equivalents)	Conditions	Yield[b] (%)
1	$Me_2CuLi{\cdot}LiI$[a] (4)	−78 °C, 30 min	95
2	$Me_2CuLi{\cdot}LiCN$[a] (4)	−78 °C, 30 min	74
3	$Me_3CuLi_2{\cdot}LiI$[a] (4)	−78 °C, 30 min	52
4	SmI_2 (6)	0 °C, 30 min	—[c]

[a] In the presence of Li salts (LiCl and/or LiBr). [b] Isolated yield. [c] A mixture of unidentified compounds was obtained.

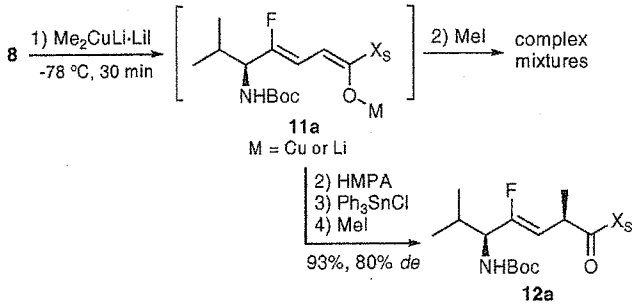

Scheme 2 Diastereoselective synthesis of a L-Val-L-Ala-type (*Z*)-fluoroalkene isostere.

Table 2 Diastereoselective synthesis of functionalized (*Z*)-fluoroalkene dipeptide isosteres by one-pot reduction/transmetalation/asymmetric alkylation

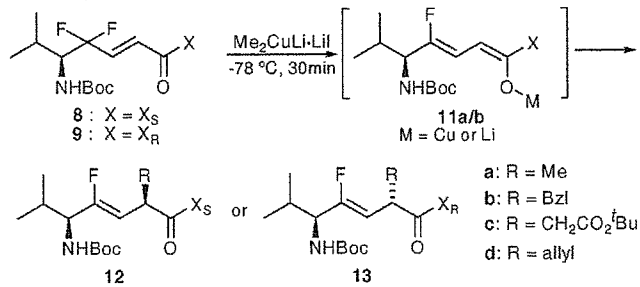

Entry	Electrophiles	Substrate	Products[a] (%)	de[b] (%)
1	MeI	**8**	**12a** (93)[c]	80
2	Bn–Br	**8**	**12b** (93)[c]	95
3	$BrCH_2CO_2{}^tBu$	**8**	**12c** (80)[c]	>95
4	Allyl–Br	**8**	**12d** (99)[c]	>95
5	$BrCH_2CH_2CO_2Me$	**8**	**10** (91)	—
6	MeI	**10**	**13a** (69)[c]	91
7	Bn–Br	**10**	**13b** (77)[c]	90
8	$BrCH_2CO_2{}^tBu$	**10**	**13c** (71)[c]	94
9	Allyl–Br	**10**	**13d** (79)[c]	92

[a] Isolated yield. [b] Determined by RP-HPLC of the purified products. [c] A trace amount of γ-alkylated products was detected by RP-HPLC.

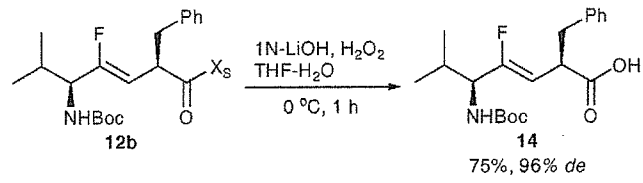

Scheme 3 Cleavage of the chiral auxiliary.

We thank Dr Terrence R. Burke Jr., NCI, NIH, USA for proofreading this manuscript. This research was supported in part by 21st Century COE Program 'Knowledge Information Infrastructure for Genome Science', a Grant-in-Aid for Scientific Research from the Ministry of Education, Culture, Sports, Science and Technology, Japan, the Japan Society for the Promotion of Science (JSPS) and the Japan Health Science Foundation.

Notes and references

‡ Fluoroalkene compounds obtained in this study have coupling constants in the range J_{HF} = 35.6–37.8 Hz. These values are consistent with those of compounds possessing (*Z*)-fluoroolefin units.[12]
§ The absolute configurations of the alkyl groups at the α-position were determined by circular dichroism measurements using an empirical rule after converting to the corresponding methyl esters.[13]

1 S. Oishi, T. Kamano, A. Niida, Y. Odagaki, N. Hamanaka, M. Yamamoto, K. Ajito, H. Tamamura, A. Otaka and N. Fujii, *J. Org. Chem.*, 2002, **67**, 6162; P. Wipf and J. Xiao, *Org. Lett.*, 2005, **7**, 103; J. Xiao, B. Weisblum and P. Wipf, *J. Am. Chem. Soc.*, 2005, **127**, 5742; H. Tamamura, K. Hiramatsu, S. Ueda, Z. Wang, S. Kusano, S. Terakubo, J. O. Trent, S. C. Peiper, N. Yamamoto, H. Nakashima, A. Otaka and N. Fujii, *J. Med. Chem.*, 2005, **48**, 380; C. L. Jenkins, M. M. Vasbinder, S. J. Miller and R. T. Raines, *Org. Lett.*, 2005, **7**, 2619.

2 R. J. Abraham, S. L. R. Ellison, P. Schonholzer and W. A. Thomas, *Tetrahedron*, 1986, **42**, 2101; T. Allmendinger, P. Furet and E. Hungerbühler, *Tetrahedron Lett.*, 1990, **31**, 7297; T. Allmendinger, E. Felder and E. Hungerbühler, *ACS Symp. Ser.*, 1991, **456**, 186; P. V. D. Veken, K. Senten, I. Kerèsz, I. D. Meester, A.-M. Lambeir, M.-B. Maes, S. Scharpè, A. Haemers and K. Augustyns, *J. Med. Chem.*, 2005, **48**, 1768; Y. Nakamura, M. Okada, A. Sato, H. Horikawa, M. Koura, A. Saito and T. Taguchi, *Tetrahedron*, 2005, **61**, 5741; A. Niida, K. Tomita, M. Mizumoto, H. Tanigaki, T. Terada, S. Oishi, A. Otaka, K. Inui and N. Fujii, *Org. Lett.*, 2006, **8**, 613.

3 A. Otaka, A. Yukimasa, J. Watanabe, Y. Sasaki, S. Oishi, H. Tamamura and N. Fujii, *Chem. Commun.*, 2003, 1834.

4 A. Otaka, E. Mitsuyama, H. Watanabe, H. Tamamura and N. Fujii, *Chem. Commun.*, 2000, 1081.

5 A. Otaka, H. Watanabe, E. Mitsuyama, A. Yukimasa, H. Tamamura and N. Fujii, *Tetrahedron Lett.*, 2001, **42**, 285; A. Otaka, H. Watanabe, A. Yukimasa, S. Oishi, H. Tamamura and N. Fujii, *Tetrahedron Lett.*, 2001, **42**, 5443.

6 A. Otaka, J. Watanabe, A. Yukimasa, Y. Sasaki, H. Watanabe, T. Kinoshita, S. Oishi, H. Tamamura and N. Fujii, *J. Org. Chem.*, 2004, **69**, 1634.

7 W. Oppolzer, D. Dupuis, G. Poli, T. M. Raynham and G. Bernardinelli, *Tetrahedron Lett.*, 1988, **29**, 5885.

8 T. Ibuka, T. Aoyagi, K. Kitada, F. Yoneda and Y. Yamamoto, *J. Organomet. Chem.*, 1985, **287**, C18; T. Ibuka, T. Aoyagi and Y. Yamamoto, *Chem. Pharm. Bull.*, 1986, **34**, 2417.

9 P. Girard, J. K. Namy and H. B. Kagan, *J. Am. Chem. Soc.*, 1980, **102**, 2693.

10 For some recent reviews, see: G. A. Molander, *Chem. Rev.*, 1992, **92**, 29; G. A. Molander, *Tetrahedron*, 1998, **54**, 3321; A. Krief and A.-M. Laval, *Chem. Rev.*, 1999, **99**, 745; P. Steel, *J. Chem. Soc., Perkin Trans. 1*, 2001, 2727.

11 P. A. Tardella, *Tetrahedron Lett.*, 1969, **10**, 1117; H. Nishiyama, K. Sakuta and K. Itoh, *Tetrahedron Lett.*, 1984, **25**, 223; H. Nishiyama, K. Sakuta and K. Itoh, *Tetrahedron Lett.*, 1984, **25**, 2487; M. Suzuki, A. Yanagisawa and R. Noyori, *J. Am. Chem. Soc.*, 1985, **107**, 3348; M. Suzuki, A. Yanagisawa and R. Noyori, *J. Am. Chem. Soc.*, 1988, **110**, 4718.

12 R. Waschüsch, J. Carran and P. Savignac, *Tetrahedron*, 1969, **52**, 14199.

13 T. Ibuka, H. Habashita, S. Funakoshi, N. Fujii, K. Baba, M. Kozawa, Y. Oguchi, T. Uehara and Y. Yamamoto, *Tetrahedron: Asymmetry*, 1990, **1**, 389.

European Journal of Neuroscience, Vol. 23, pp. 1120–1128, 2006 doi:10.1111/j.1460-9568.2006.04646.x

HIV-1 gp120 enhances giant depolarizing potentials via chemokine receptor CXCR4 in neonatal rat hippocampus

Alexander Kasyanov,[1,2] Hirokazu Tamamura,[3] Nobutaka Fujii[4] and Huangui Xiong[1,2]
[1]Neurophysiology Laboratory, Center for Neurovirology and Neurodegenerative Disorders, University of Nebraska Medical Center, Omaha, USA
[2]Department of Pharmacology and Experimental Neuroscience, University of Nebraska Medical Center, Omaha, NE 68198–5880, USA
[3]Department of Molecular Recognition, Institute of Biomaterials and Bioengineering, Tokyo Medical and Dental University, Tokyo, Japan
[4]Graduate School of Pharmaceutical Sciences, Kyoto University, Kyoto, Japan

Keywords: brain slices, EPSPs, HIV, patch clamp, Sprague–Dawley rat

Abstract

In the immature hippocampus, the giant depolarizing potentials (GDPs) are recurrent network-driven synaptic events generated by γ–aminobutyric acid (GABA), which in neonatal life is depolarizing and excitatory. The GDPs enable a high degree of synchrony in immature neurons and participate in activity-dependent growth and synapse formation. To understand how human immunodeficiency virus type one (HIV-1) infection in the immature brain impairs brain growth and development, we studied the effects of HIV-1 envelope glycoprotein, gp120, a viral toxin shed in abundance by infected cells, on spontaneous occurring GDPs recorded in the CA3 pyramidal cells in neonatal (P2–P6) Sprague–Dawley rat hippocampal slices using whole-cell patch technique. Bath application of gp120 produced a sustained enhancement of GDP frequency in a concentration-dependent manner without affecting passive membrane properties, suggesting that the site of action is most likely on neural network, other than on the recorded neurons. The gp120-induced enhancement of GDPs was blocked by T140, a highly specific antagonist for the chemokine receptor, CXCR4, indicating the involvement of CXCR4 in the gp120-induced increase of GDPs. Bath application of stromal cell-derived factor-1α (SDF-1α), the only CXCR4 ligand, mimicked the effects of gp120 on GDPs, supporting the engagement of CXCR4 receptors in the gp120-induced increase of GDP occurrence. Further studies revealed the involvement of protein kinase A/C in the gp120-induced enhancement of GDPs. These results demonstrate that gp120 enhances GDPs in the neonatal rat hippocampus. This enhancement may cause an excessive increase in intracellular calcium and resultant neuronal injury, leading to retardation of the brain and behavioural development as seen in paediatric AIDS patients.

Introduction

Infants and young children infected with human immunodeficiency virus type one (HIV-1) often have a higher incidence of HIV-1-associated encephalopathy (HE), a devastating complication of HIV-1 infection in the central nervous system (CNS; Ammann, 1994; Belman, 1994). HE is manifested as a well-defined triad of clinical features, i.e. impaired brain growth, loss of developmental milestones with cognitive deterioration, and symmetrical motor deficit (Epstein *et al.*, 1986; Belman *et al.*, 1988; Mintz & Epstein, 1992). A recent large cohort study revealed that approximately 10% of children developed HE during the first year of HIV-1 infection (in contrast to 0.3% in adults) and cumulative incidence at seven years postinfection reached 16% in children and 5% in adults (Tardieu *et al.*, 2000). The frequent occurrence of HE in these young patients adds significantly to the morbidity of the disease (Belman *et al.*, 1993). Nevertheless, the mechanisms underlying clinical onset of HE in children remain unknown. It is commonly believed that the pathogenesis of HE in paediatric patients is similar to the pathophysiologic mechanisms of HIV-1-associated dementia (HAD) in adult patients, involving viral infection, immune activation of brain mononuclear phagocytes (MPs, brain macrophages and microglia), and resultant release of diffusible viral and cellular toxins, leading to neuronal and astrocytic dysfunction and/or death (Gendelman *et al.*, 1997; Nath, 2002). Amongst these toxins is the HIV-1 envelope glycoprotein, gp120, one of the major viral toxins released from HIV-1-infected MPs. Accumulating evidence suggests that gp120 plays an important role in HIV-1-associated neuropathology in HAD and HE.

HIV-1 gp120 induces neurotoxic activity in cultures of rodent hippocampal and human embryonic neurons (Dawson *et al.*, 1993; Lannuzel *et al.*, 1995; Meucci & Miller, 1996), as well as in rodent brains *in vivo* (Bagetta *et al.*, 1996b; Bansal *et al.*, 2000). Systemic administration of gp120 in neonatal rats or intracerebroventricular injection in adult rats resulted in deleterious effects on the brain (Hill *et al.*, 1993; Bagetta *et al.*, 1996a; Acquas *et al.*, 2004). Overexpression of gp120 in the brains of transgenic mice produced widespread neuronal dendritic vascularization and loss of neuronal populations (Toggas *et al.*, 1994). Thus, gp120 has been proposed to

Correspondence: Dr Huangui Xiong, [2]Department of Pharmacology and Experimental Neuroscience, as above.
E-mail: hxiong@unmc.edu

Received 24 August 2005, revised 21 December 2005, accepted 23 December 2005

be the major aetiologic agent inducing neuronal cell dysfunction or death and other debilitating neurological and behaviour consequences of HIV-1 infection observed in HAD and HE. Gp120 causes neuronal damage by stimulating MP to release neurotoxins such as cytokines and chemokines. It may also act on neuronal cells directly by binding to neuronal CXCR4 receptors (Horuk *et al.*, 1997; Kaul *et al.*, 2001), producing an increase in intracellular free calcium concentration $[Ca^{2+}]_i$ (Dreyer *et al.*, 1990; Medina *et al.*, 1999). Interestingly, gp120 was found to induce two different types of $[Ca^{2+}]_i$ oscillation in primary hippocampal neuronal cultures. One type of $[Ca^{2+}]_i$ oscillation required the maintained presence of gp120 and ceased when gp120 was removed from the bath, and the other type of oscillations persisted long after washout of gp120 (Lo *et al.*, 1992). The gp120-induced $[Ca^{2+}]_i$ oscillations were completely blocked by antagonists of Na^+ and NMDA-gated ion channels, suggesting that they might be mediated via network-driven synaptic events (Lo *et al.*, 1992).

In immature brains, spontaneously occurring neuronal oscillations constitute a hallmark of developmental networks and participate in activity-dependent brain growth and synapse formation (Ben-Ari, 2001). These neuronal oscillations, so-called 'giant depolarizing potentials' (GDPs), result in calcium influx through NMDA receptor channels and voltage-gated calcium channels (Khazipov *et al.*, 1997). However, uncontrolled and excessive accumulation of $[Ca^{2+}]_i$ is considered as the unifying theme in a number of cytotoxic processes that lead to neuronal dysfunction and apoptosis (Hesselgesser *et al.*, 1998). To understand how HIV-1 alters neuronal function in the developing nervous system, we studied the effects of HIV-1 gp120 on GDPs recorded in the CA3 pyramidal cells in neonatal rat hippocampal slices. We found that gp120 enhanced GDP frequency through CXCR4, a chemokine receptor expressed in both glial cells (astrocyte and microglia) and specific subsets of neurons (Asensio & Campbell, 1999). An abstract form of these results was presented at the 2004 Society for Neuroscience 34th Annual Meeting in San Diego, CA, USA.

Materials and methods

Materials

HIV-1 $gp120_{MN}$ was obtained from the National Institute of Health (NIH) AIDS Research and Reference Reagent Program (Rockville, MD, USA). Aliquots of gp120 were kept as 200 ng/μL stock solution at −80 °C. The stock solution was diluted to the desired concentrations with artificial cerebrospinal fluid (ACSF) 2–5 min before application. Stromal cell-derived factor-1α (SDF-1α) was purchased from R & D Systems (Minneapolis, MN, USA). Fura-2 AM was obtained from Molecular Probes (Eugene, OR, USA). Neurobasal media was purchased from Invitrogen Corp (Carlsbad, CA, USA). T140 was obtained from Kyoto University (Sakyo-ku, Kyoto, Japan). All chemicals, unless otherwise specified, were from Sigma (St. Louis, MO, USA).

Primary hippocampal-cortical neuronal cultures

Pregnant Sprague-Dawley rats were anaesthetized with isoflurane and embryonic rats (17–18-day-old) were dissected out under sterile conditions. The fetal rats were decapitated and hippocampal and cortical tissues collected. Individual cells were mechanically dissociated by trituration in a Ca^{2+}/Mg^{2+}-free Hank's balanced salt solution (HBSS) after 30 min of trypsin (0.1%) digestion at 37 °C. Trypsin was neutralized with 10% fetal bovine serum (FBS, 10%) and the cell suspension washed three times in HBSS and resuspended in neurobasal medium (Invitrogen Corp, Carlsbad, CA, USA) supplemented with 2 mM glutamine, 50 μg/mL penicillin and streptomycin and B27. Cells were seeded in poly D-lysine coated cover slips at a concentration of 250 000 cells/mL. The cells were used for Ca^{2+} imaging after 12–14 days in culture.

Calcium flux analysis

Cells were loaded with 5 μM Fura-2 AM using the procedure as previously described. Fura-2 fluorescence was imaged with an inverted Nikon TMD Diaphot epifluorescent microscope (40× water immersion lens). The change in free Ca^{2+} was measured by monitoring the intensity of excitation emission at 510 nm in response to repeated sequential excitation at 340 nm and 380 nm using a digital camera (Photometrics, Huntington Beach, CA). Excitation control, image acquisition and off-line analysis of images were performed using Axon Imaging Workbench-2 (Axon Instruments). The selection of neuronal cells for Ca^{2+} imaging was based on cell morphology and the selected cells in the image were analysed independently for each time point in the captured sequence. Data are presented as the relative ratio of fluorescence at 340 nm and 380 nm.

Hippocampal brain slice preparation

Hippocampal brain slices were prepared from postnatal day 2 (P2) to P6 Sprague–Dawley rats of either sex as described previously (Kasyanov *et al.*, 2004). Briefly, rats were anaesthetized with isoflurane and decapitated. The brain was quickly removed from the skull and submerged in ACSF containing (in mM): NaCl 126, KCl 3.5, $CaCl_2$ 2, $MgCl_2$ 1.3, NaH_2PO_4 1.2, $NaHCO_3$ 25, glucose 11, and saturated with 95% O_2 and 5% CO_2 (pH 7.3–7.4). Coronal hippocampal slices (500 μm in thickness) were cut with a vibrating microslicer (World Precision Instruments, Sarasota, FL, USA) and incubated at room temperature in oxygenated ACSF for at least 1 h before use. Individual slices were transferred to the recording chamber and superfused with ACSF at 2.5–3.0 mL/min at 34 °C. The Institutional Animal Care and Use Committee (IACUC) of University of Nebraska Medical Center strictly reviewed all animal use procedures (IACUC # 00-062-07).

Electrophysiology and data analyses

Whole-cell current-clamp recordings were performed on CA3 pyramidal cells in hippocampal slices using a 'blind' method. Spontaneous GDPs and excitatory postsynaptic potentials (EPSPs) were recorded and amplified using an Axopatch-1D amplifier (Axon Instruments, Union City, CA, USA), filtered at 1 kHz, and digitized at 5 kHz through a Digidata 1322A (Axon Instruments). To minimize potential 'contamination' of the EPSPs by spontaneous action potentials, the cells were hyperpolarized to −80 mV PCLAMP 8 software (Axon Instruments) was used for data acquisition (gap-free configuration) and the data was stored in a PC computer. The patch electrodes were made from borosilicate glass capillaries (World Precision Instruments) and had a resistance of 5–7 MΩ when filled with intracellular solution containing (in mM): KCl 140, HEPES 10, EGTA 1, $MgCl_2$ 1, MgATP 2 (pH 7.3 with KOH, osmolarity 280–290 mOsm). The whole cell capacitance was fully compensated and the series resistance (10–20 MΩ) was compensated at 75–80%. Membrane input resistance was calculated by measuring membrane voltage change in response to small hyperpolarizing current pulses (300 ms in duration) across the cell membrane. Series resistance was monitored throughout the recordings. A cell was discarded if it changed significantly (> 20% of the control). Both PCLAMP 8 and Mini Analysis Program

(Synaptosoft Inc, Decatur, GA, USA) were employed for data analyses. For each cell, the mean GDP frequency was calculated before (control), during (starting 1 min after the onset of drug perfusion) and after (washout) drug application. Statistical comparisons were made between mean values (control vs. drug treatment). The numerical data are given as mean ± SD and compared using the Student's *t*-test or Kolmogorov–Smirnov (K–S) test. The differences were considered significant when $P < 0.05$.

Results

HIV-1 gp120 increases GDP frequency in CA3 pyramidal cells

To understand how HIV-1 gp120 affects neuronal activity in developing nervous system, we studied the effects of HIV-1 gp120 on GDPs recorded from CA3 pyramidal cells in hippocampal brain slices taken from neonatal rats (P2–P6). Under whole-cell current clamp, the CA3 pyramidal cells fire spontaneous GDPs. The occurrence of GDPs was random and independent of cell membrane potential, with an average firing frequency of 0.088 ± 0.015 Hz ($n = 26$). The spontaneous GDPs were blocked either by the $GABA_A$ receptor antagonist, picrotoxin, (100 μM, $n = 5$) or by the Na^+ channel blocker, tetrodoxin (TTX, 0.1 μM, $n = 4$), but not by the NMDA receptor antagonist, 2-amino-5-phosphovalerate (APV, 50 μM, $n = 4$, data not shown). These results suggest that GDPs were GABA-mediated, network-driven events. In order to evaluate whether HIV-1 gp120 affects GDP occurrence, we exposed hippocampal brain slices to gp120 through bath perfusion. Bath application of gp120 produced a long-lasting enhancement of GDP firing frequency in CA3 pyramidal cells in a concentration-dependent manner (Fig. 1). When slices were perfused with gp120 at concentrations of 2, 20, and 200 pM, respectively, the average GDP frequency (Hz) was from 0.095 ± 0.010 to 0.089 ± 0.010 ($n = 3$), 0.123 ± 0.003 to 0.152 ± 0.006 ($n = 3$), and 0.045 ± 0.003 to 0.071 ± 0.002 Hz ($n = 6$), respectively (Fig. 1D). The enhancement occurred 3–5 min after gp120 reached the recording chamber and lasted for >15 min during the washout period (Fig. 1A–C). While it enhanced the occurrence of GDPs, gp120 had no significant ($P > 0.05$, $n = 5$) effects on spontaneous mini EPSPs. The average mini-EPSP occurring frequency was 3.6 ± 1.3 Hz in control, 3.6 ± 1.1 Hz during application of gp120, and 2.8 ± 0.7 Hz during the wash period (Fig. 2; $n = 5$). Application of gp120 did not

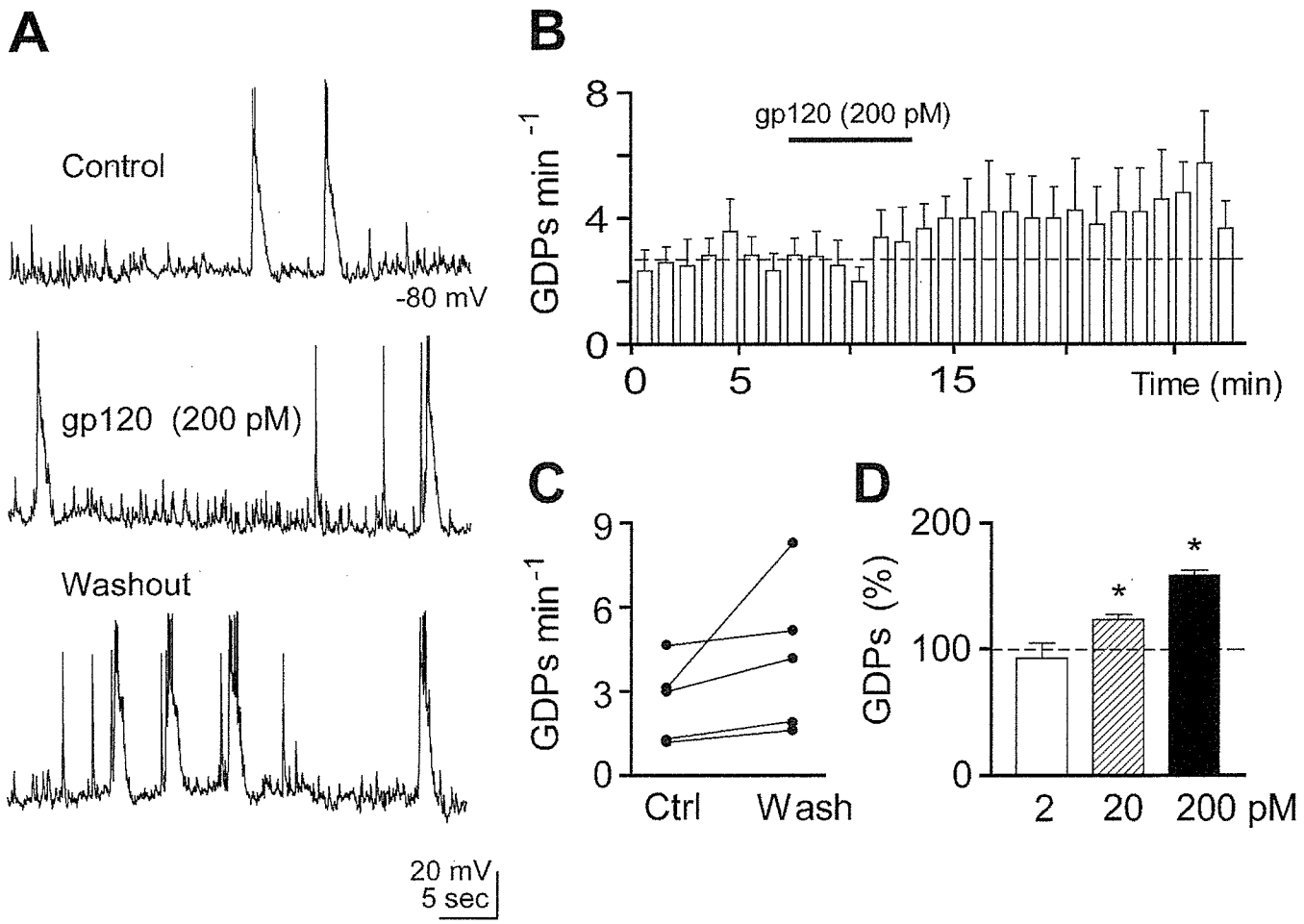

FIG. 1. HIV-1 gp120 produces persistent enhancement of GDP firing frequency. Panel A shows the representative traces recorded under current clamp from a CA3 pyramidal neuron (P4) under control (upper), during bath application of gp120 (middle), and 5 min after washout started (lower). Note the increase of GDP firing during the washout period. Panel B is the time course illustrating the average GDP frequency before, during, and after gp120 application ($n = 5$). Each bar represents the number of GDPs recorded in 1 min. The dotted line represents the mean GDP frequency under control conditions. The horizontal bar indicates bath application of gp120 (200 pM). Panel C plots GDP frequencies recorded from five individual cells (as shown in panel B) during control and 5 min after washout started. Panel D is a summarized bar graph illustrating the relationship of average GDP frequency as a function of gp120 concentrations. Each bar represents the percentage of changing of the GDP frequency induced by gp120 at 2, 20, 200 pM, respectively. *$P < 0,05$

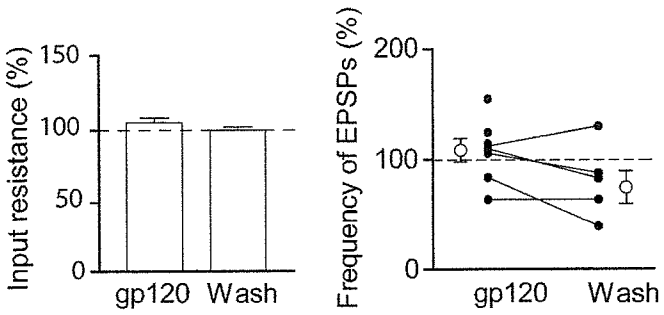

FIG. 2. HIV-1 gp120 had no significant effects on membrane input resistance (A) and spontaneous EPSPs (B). The membrane input resistance (A) was 103.2 ± 3.2% of control level (dashed line) during bath perfusion of gp120 and 97.9 ± 2.0% of control level during washout period. Panel B shows the spontaneous EPSP frequency recorded from individual neurons during bath application of gp120 (n = 7, filled circles) and 5 min after the start of wash (n = 5, filled circles), expressed as percentage of control level (dashed line). The open circles represent the average EPSP frequency during bath application of gp120 (left) and 5 min after the start of wash (right).

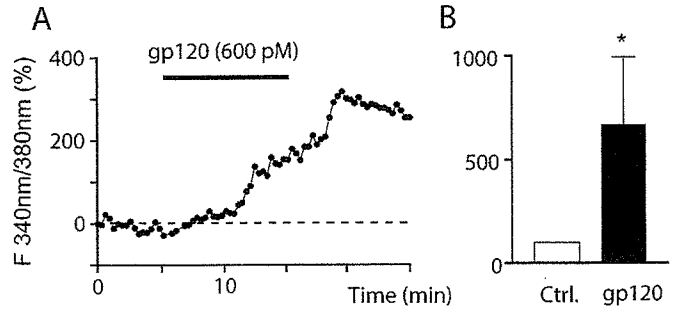

FIG. 3. gp120 evoked an increase of intracellular Ca^{2+} concentration in fetal rat hippocampal-cortical neuronal cultures. Panel A (left) shows an example of the change of fluorescence ratio in response to bath application of gp120 (600 pM). Panel B (right) illustrates the average of fluorescence ratio measured before (Ctrl) and 10 min after bath application of gp120 (gp120, n = 4). Note that gp120 induced a significant increase of the relative ratio of fluorescence at 340 and 380 nM, suggesting a rise of intracellular Ca^{2+} concentration induced by gp120.

produce a significant change in either cell resting membrane potential, or cell membrane input resistance. The average resting membrane potentials before, during, and after application of gp120 were 89 ± 7 mV, 95 ± 8 mV, and 92 ± 12 mV, respectively (n = 6). The average membrane input resistance was 103.2 ± 3.2% of the basal level (n = 3) during bath application of gp120 and 97.9 ± 2.0% of the basal level (n = 3) when measured during the wash period (Fig. 2).

Gp120 induces a persistent increase in intracellular calcium in neurons

GDPs increase the levels of $[Ca^{2+}]_i$ through activation of voltage-gated Ca^{2+} channels (Leinekugel *et al.*, 1995) and/or by reducing the voltage-dependent Mg^{2+} blockade of NMDA receptor channels and resultant activation of NMDA receptors, resulting in a further rise of $[Ca^{2+}]_i$ (Leinekugel *et al.*, 1997). We hypothesized that the enhancement of GDP frequency by gp120 may cause substantial increase of intracellular Ca^{2+} levels. To test this hypothesis, we measured $[Ca^{2+}]_i$ in primary fetal rat hippocampal-cortical neuronal cultures. Utilizing the single cell calcium imaging system at the Center for Neuroviology and Neurodegenerative Disorders, we indeed demonstrated in four out of ten cells a profound calcium response in the presence of gp120 (Fig. 3), with an average fluorescence ratio of 668 ± 326% (mean ± SD, n = 4). In comparison with the fluorescence ratio detected in untreated controls, the difference is statistically significant ($P < 0.05$), suggesting that gp120 increases GDP frequency and intracellular Ca^{2+} levels.

Blockade of gp120-induced enhancement of GDPs by T140, an antagonist for chemokine receptor CXCR4

Gp120 interacts with CXCR4 receptors and the receptors have been detected in human fetal neuronal and glial cell cultures (Zheng *et al.*, 1999; Croitoru-Lamoury *et al.*, 2003), and in neurons from autopsy brain tissues in children (Vallat *et al.*, 1998) and adults (Lavi *et al.*, 1997; Lavi *et al.*, 1998). To examine if the gp120-induced increase of GDP occurrence is mediated through activation of chemokine receptor CXCR4, we tested the effects of T140, a highly selective CXCR4 receptor antagonist that has recently been shown to strongly suppress HIV-1 entry into target cells by blocking viral gp120 binding to CXCR4 receptors (Tamamura & Fujii, 2004), on gp120-induced enhancement of GDP occurrence. While it had no significant effect on spontaneous GDP occurrence when applied by bath (Fig. 4A; n = 5), T140 (50 nM) significantly blocked gp120-induced enhancement of GDP frequency (Fig. 4A and B; n = 5). The blockade of gp120-induced enhancement of spontaneous GDPs by CXCR4 receptor

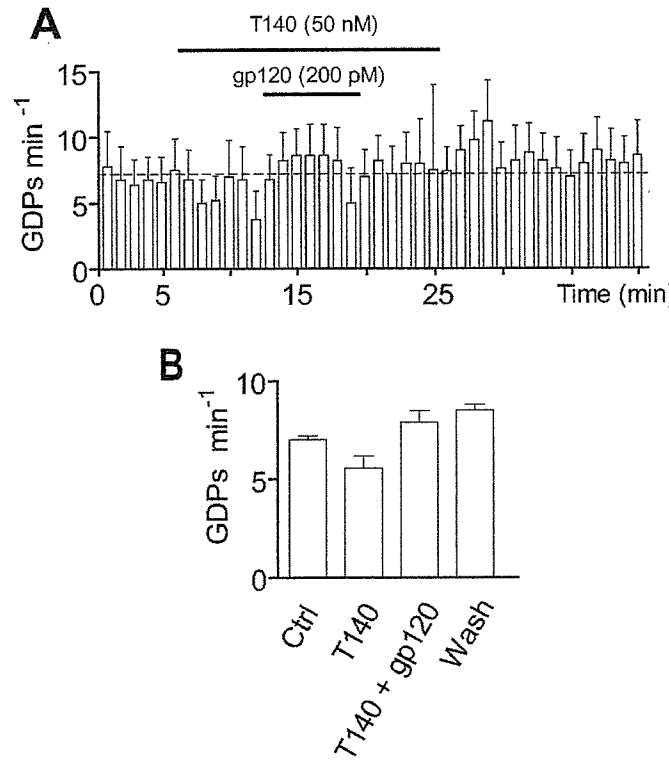

FIG. 4. Blockade of the HIV-1 gp120-induced enhancement of GDP occurrence by T140, a specific CXCR4 receptor antagonist. (A) Time course showing the averaged GDP firing frequency for five cells. Each column represents the number of GDPs recorded in 1 min. The dotted line represents the mean GDP frequency under control conditions. Note that gp120 failed to increase GDP frequency in the presence of T140. (B) Each bar represents the mean GDP frequency observed in five neurons during control, application of T140 (50 nM, before gp120 application), T140 plus gp120 (200 pM), and wash. Error bars represent the SEM.

antagonist suggests that gp120 increases GDP frequency through CXCR4 receptors.

SDF-1α mimics the effects of gp120 on the GDP

To explore further whether gp120-induced enhancement of GDP frequency occurs through CXCR4 receptors, we examined the effects of SDF-1α, the only ligand for CXCR4 receptors, on GDP frequency in CA3 pyramidal cells. Bath application of SDF-1α (50 nM) induced biphasic effects on GDP firing frequency, with an initial decrease from 0.115 ± 0.007 Hz to 0.064 ± 0.014 Hz followed by a significant increase from 0.115 ± 0.007 Hz to 0.142 ± 0.006 Hz (Fig. 5A–C; $n = 5$) during the wash period. The depressive effect of SDF-1α was rapid in onset, reaching maximum effect in 2–3 min, and the recovery was attained 3–5 min after starting the washout (Fig. 5B). SDF-1α did not alter the resting membrane potential, membrane input resistance, or the shape of GDPs. The membrane potentials before, during, and after application of SDF-1α were −80 ± 6 mV, −80 ± 5 mV, and −85 ± 1 mV, respectively. Membrane input resistance were 99.1 ± 7.2% of the basal level during application of SDF-1α and 107 ± 18.7% of the basal level during the wash period ($n = 3$). The differences were not statistically significant ($P > 0.05$). Like gp120, SDF-1α did not produce significant effects on spontaneous mini-EPSPs, with an average frequency of 1.43 ± 0.34 Hz in control and 1.61 ± 0.27 Hz during application of SDF-1α ($n = 3$, $P > 0.05$, K–S test). These results demonstrated that SDF-1α mimicked the effects of gp120 on GDPs, providing further evidence supporting our hypothesis that gp120 increases GDP frequency through CXCR4 receptors.

H7 blocked the effects of gp120 on GDPs

It has been shown that gp120 activates protein kinase C (PKC) in the hippocampus (Zorn *et al.*, 1990) and induces apoptosis in primary endothelium through PKC (Huang & Bond, 2000). We hypothesize that gp120 may increase GDP frequency through activation of PKC and/or cAMP-dependent protein kinase (PKA). To test this hypothesis, we examined the effects of H7, an inhibitor for PKA and PKC, on gp120-induced enhancement of GDP occurrence in neonatal hippocampal slices. When applied alone, H7 (100 μM) inhibited GDP occurrence ($n = 4$), showing the involvement of PKA and/or PKC in the occurrence of spontaneous GDPs. However, when coapplied with gp120, H7 blocked the gp120-associated increase of GDP frequency (Fig. 6A). The average GDP frequency before (control) and after coapplication of H7 and gp120 were 0.080 ± 0.005 Hz and 0.060 ± 0.003 Hz ($n = 4$), respectively. In comparison with the GDP frequency occurred after bath application of gp120 (Fig. 1D), the difference was statistically significant ($P < 0.05$), suggesting the involvement of PKA/PKC in gp120-induced increase of GDPs. To verify whether activation of PKA enhances GDPs, we tested the effects of the adenylyl cyclase stimulator, forskolin, on GDP frequency. Our results showed that forskolin mimicked the effects of gp120 on GDPs (Fig. 6B), illustrating that the cAMP-dependent protein kinase may also be involved in gp120-induced enhancement of GDPs. Taken together, these results suggest that gp120 increases GDP firing frequency through a CXCR4 receptor-PKA/C signal pathway.

Discussion

In this study, we demonstrated that the HIV-1 envelope glycoprotein, gp120, induced a persistent increase of network-driven, GABA-mediated GDP firing frequency in the CA3 pyramidal cells in neonatal rat hippocampal slices. HIV-1 gp120 enhances neuronal spontaneous GDP firing frequency in a concentration-dependent manner without affecting the neuronal resting membrane potential and membrane input resistance, suggesting that the site of action for gp120 is most likely on the neural network, other than on the neurons recorded. The

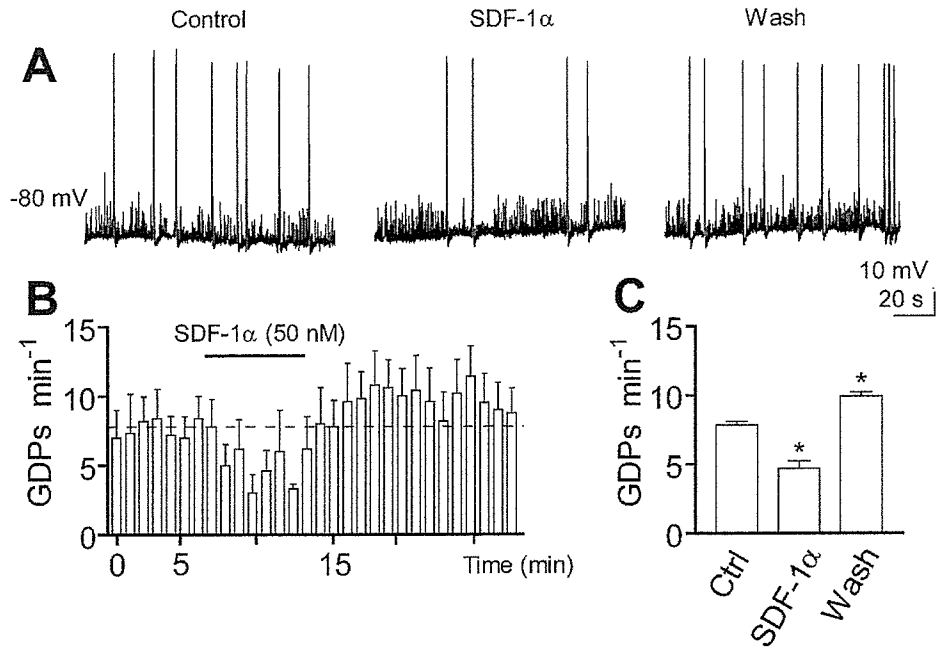

FIG. 5. SDF-1α, the only ligand for the chemokine receptor, CXCR4, modulates the GDP firing frequency. (A) Representative spontaneous GDPs recorded from a CA3 pyramidal neuron at P3 before (control), during (SDF-1α) and after (wash) bath application of SDF-1α (50 nM). (B) Time course showing the effects of SDF-1α on spontaneous GDP frequency ($n = 5$). Each column represents the number of GDPs recorded in 1 min. The dotted line represents the mean GDP frequency under control conditions. (C) The bar graph depicts the average GDP frequencies sampled before, during, and after SDF-1α application. Data represent mean ± SD from five neurons. *$P < 0.05$ when compared with Ctrl.

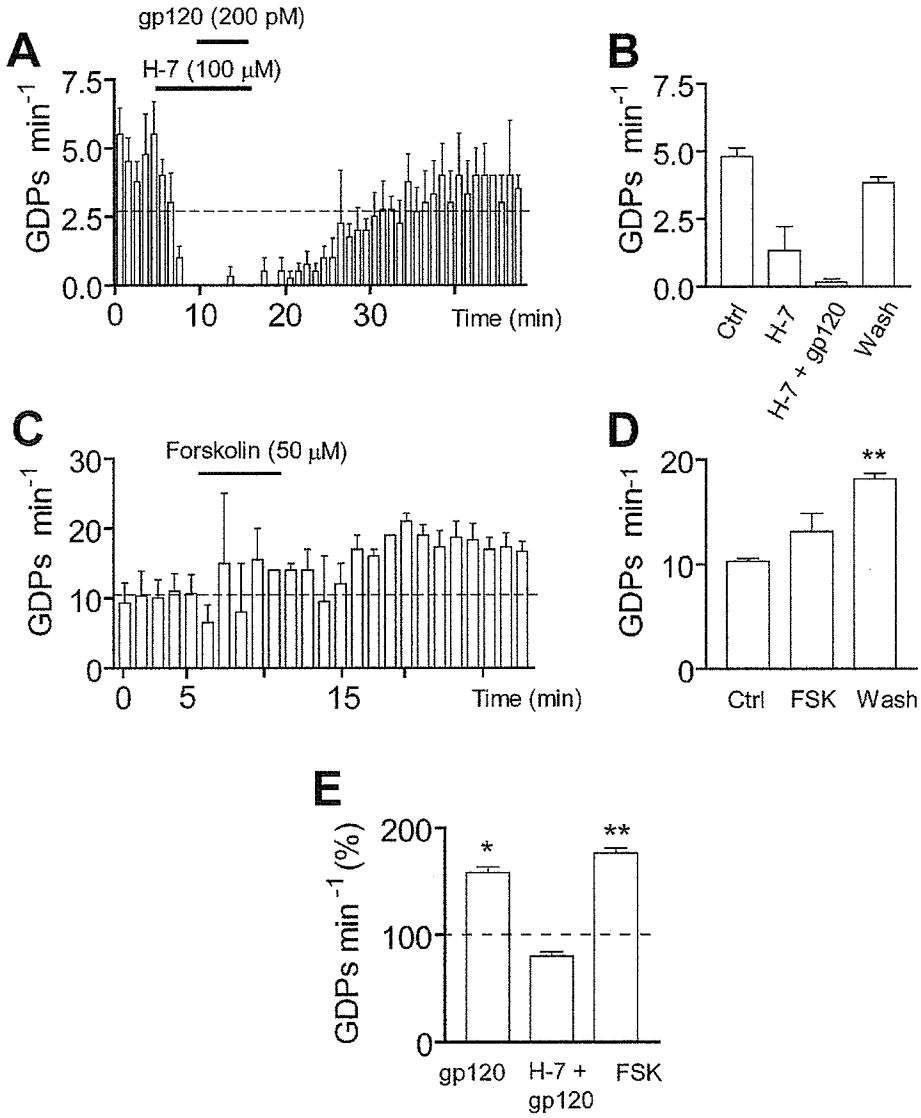

FIG. 6. Involvement of protein kinase A/C in gp120-induced enhancement of GDP firing. Panel A is the time course showing the average GDP firing frequency for five cells. Each column represents the number of GDPs recorded in 1 min. The dotted line represents the mean GDP frequency under control condition. Bath application of H7 inhibited GDP occurrence and blocked gp120-associated enhancement of GDPs. The average frequencies taken from control, during applications of H7 and H7 + gp120, and washout period are presented as a bar graph (B). Note gp120 failed to enhance GDPs in the presence of H7 in the perfusate. Panels C and D illustrate that activation of adenylyl cyclase by forskolin mimicked the effect of gp120 on GDPs, suggesting the possible involvement of PKA in gp120 enhancement of GDPs. A comparison of average GDP frequencies taken during washout periods following bath application of gp120, H7 + gp120 and forskolin are shown in panel E. Note that H7 blocked and forskolin mimicked the effects of gp120 on GDPs. $^{*}P < 0.05$; $^{**}P < 0.01$.

gp120-induced enhancement of GDP frequency was blocked by a highly specific CXCR4 receptor antagonist, T140, indicating the involvement of CXCR4 receptors in the gp120-associated increase of GDP frequency. Application of SDF-1α, the only ligand for CXCR4, mimicked the effects of gp120 on GDPs, further supporting our finding that gp120 increases GDP occurrence through CXCR4 receptors. The involvement of PKA/PKC in gp120-induced enhancement of GDPs was confirmed by bath application of H7, an antagonist for PKA/PKC.

HIV-1 gp120 is toxic to neurons and causes neural cell death at very low concentrations *in vitro* (Brenneman *et al.*, 1988; Dreyer *et al.*, 1990). In HIV-1-infected brain, gp120 is shed from virions and has the potential to diffuse and interact directly with surrounding and distant neural cells through activation of CXCR4 receptors (Hesselgesser *et al.*, 1998; Meucci *et al.*, 1998; Acquas *et al.*, 2004; Bachis & Mocchetti, 2004), or by stimulating uninfected macrophage-glial cells to release toxins that act indirectly on local and distant neural cells, or both. Treatment of human or rat neurons in culture with gp120 leads to neuronal apoptosis (Bachis & Mocchetti, 2004; Brenneman *et al.*, 1988; Meucci *et al.*, 1996) and intracerebroventricular injection of gp120 in rats produces apoptotic neuronal death *in vivo* (Bagetta *et al.*, 1996b; Acquas *et al.*, 2004). Transgenic mice expressing the HIV-1 gp120 manifest a spectrum of neuronal and glial changes resembling abnormalities in brains of HIV-1-infected humans and the severity of damage correlated positively with the brain levels of gp120 expression (Toggas *et al.*, 1994). Our results showed that gp120 enhances GDP frequency without significant influence on neuronal resting membrane potential, membrane input resistance and spontaneous EPSPs. This suggests that gp120 most likely alters GDP frequency by acting on other cellular elements in the hippocampus